Inorganic Chemistry

Article

pubs.acs.org/IC

Synthesis, Structure, Luminescent, and Magnetic Properties of Carbonato-Bridged $Zn^{II}_2Ln^{III}_2$ Complexes $[(\mu_4\text{-}CO_3)_2\{Zn^{II}L^nLn^{III}(NO_3)\}_2]$ (Ln^{III} = Gd^{III}, Tb^{III}, Dy^{III}; L^1 = *N*,*N*′-Bis(3-methoxy-2-oxybenzylidene)-1,3-propanediaminato, L^2 = *N*,*N*′-Bis(3-ethoxy-2-oxybenzylidene)-1,3-propanediaminato)

Kiyomi Ehama,[†] Yusuke Ohmichi,[†] Soichiro Sakamoto,[†] Takeshi Fujinami,[†] Naohide Matsumoto,*[,†] Naotaka Mochida,[‡] Takayuki Ishida,[‡] Yukinari Sunatsuki,[§] Masanobu Tsuchimoto,[∥] and Nazzareno Re[⊥]

[†]Department of Chemistry, Faculty of Science, Kumamoto University, Kumamoto 860-8555, Japan

[‡]Department of Engineering Science, The University of Electro-Communications, Chofu, Tokyo 182-8585, Japan

[§]Department of Chemistry, Faculty of Science, Okayama University, Tsushima-naka 3-1-1, Okayama 700-8530, Japan

[∥]Department of Chemistry, Chiba Institute of Technology, Shibazono 2-1-1, Narashino, Chiba 275-0023, Japan

[⊥]Facolta di Farmacià, Universita degli Studi "G. d'Annunzio", I-66100 Chieti, Italy

Supporting Information

ABSTRACT: Carbonato-bridged $Zn^{II}_2Ln^{III}_2$ complexes $[(\mu_4\text{-}CO_3)_2\{Zn^{II}L^nLn^{III}(NO_3)\}_2]\cdot$solvent were synthesized through atmospheric CO_2 fixation reaction of $[Zn^{II}L^n(H_2O)_2]\cdot xH_2O$, $Ln^{III}(NO_3)_3\cdot 6H_2O$, and triethylamine, where Ln^{III} = Gd^{III}, Tb^{III}, Dy^{III}; L^1 = *N*,*N*′-bis(3-methoxy-2-oxybenzylidene)-1,3-propanediaminato, L^2 = *N*,*N*′-bis(3-ethoxy-2-oxybenzylidene)-1,3-propanediaminato. Each $Zn^{II}_2Ln^{III}_2$ structure possessing an inversion center can be described as two di-μ-phenoxo-bridged $\{Zn^{II}L^nLn^{III}(NO_3)\}$ binuclear units bridged by two carbonato CO_3^{2-} ions. The Zn^{II} ion has square pyramidal coordination geometry with N_2O_2 donor atoms of L^n and one oxygen atom of a bridging carbonato ion at the axial site. Ln^{III} ion is coordinated by nine oxygen atoms consisting of four from the deprotonated Schiff-base L^n, two from a chelating nitrate, and three from two carbonate groups. The temperature-dependent magnetic susceptibilities in the range 1.9−300 K, field-dependent magnetization from 0 to 5 T at 1.9 K, and alternating current magnetic susceptibilities under the direct current bias fields of 0 and 1000 Oe were measured. The magnetic properties of the $Zn^{II}_2Ln^{III}_2$ complexes are analyzed on the basis of the dicarbonato-bridged binuclear Ln^{III}−Ln^{III} structure, as the Zn^{II} ion with d^{10} electronic configuration is diamagnetic. **ZnGd1** (L^1) and **ZnGd2** (L^2) show a ferromagnetic Gd^{III}−Gd^{III} interaction with J(Gd−Gd) = +0.042 and +0.028 cm^{-1}, respectively, on the basis of the Hamiltonian $\mathbf{H} = -2J(\text{Gd}-\text{Gd})\hat{\mathbf{S}}_{Gd1}\cdot\hat{\mathbf{S}}_{Gd2}$. The magnetic data of the $Zn^{II}_2Ln^{III}_2$ complexes (Ln^{III} = Tb^{III}, Dy^{III}) were analyzed by a spin Hamiltonian including the crystal field effect on the Ln^{III} ions and the Ln^{III}−Ln^{III} magnetic interaction. The Stark splitting of the ground state was so evaluated, and the energy pattern indicates a strong easy axis (Ising type) anisotropy. Luminescence spectra of $Zn^{II}_2Tb^{III}_2$ complexes were observed, while those of $Zn^{II}_2Dy^{III}_2$ were not detected. The fine structure assignable to the $^5D_4 \rightarrow {}^7F_6$ transition of **ZnTb1** and **ZnTb2** is in good accord with the energy pattern from the magnetic analysis. The $Zn^{II}_2Ln^{III}_2$ complexes (Ln^{III} = Tb^{III}, Dy^{III}) showed an out-of-phase signal with frequency-dependence in alternating current susceptibility, indicative of single molecule magnet. Under a dc bias field of 1000 Oe, the signals become significantly more intense and the energy barrier, Δ/k_B, for the magnetic relaxation was estimated from the Arrhenius plot to be 39(1) and 42(8) K for **ZnTb1** and **ZnTb2**, and 52(2) and 67(2) K for **ZnDy1** and **ZnDy2**, respectively.

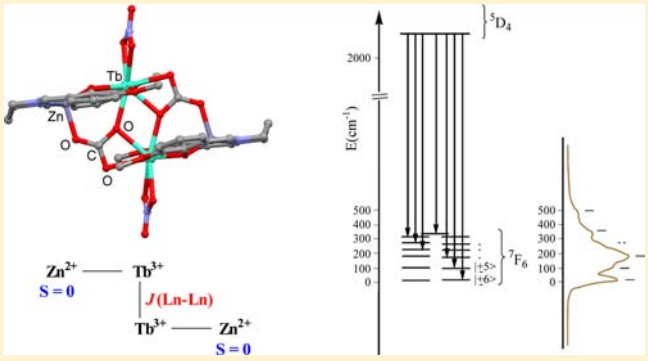

INTRODUCTION

The discovery of the SMM (single molecule magnet) properties of a Mn_{12} cluster in the 1990s is recognized as a breakthrough in the history of magnetism.[1] Since then, the number of SMMs consisting of d-element has been studied[2] and it was revealed that the SMM behavior is originated from the easy axis magnetic anisotropy (D < 0) of a large spin molecule, which causes the formation of an energy barrier that prevents reversal of the molecular magnetization. Subsequently, it was found that d−f

Received: September 1, 2013
Published: October 23, 2013

 © 2013 American Chemical Society dx.doi.org/10.1021/ic4022273 | *Inorg. Chem.* 2013, 52, 12828−12841

polynuclear and radical−f complexes may give a valuable contribution to the molecular design of SMMs,[3] because large spin ground states can be generated by ferromagnetic interaction frequently observed between d- and f-elements, and a large molecular magnetic anisotropy can be easily derived from the f-component. In 2003, Ishikawa reported that phthalocyaninato lanthanide complexes exhibit slow relaxation of the magnetization, and that a lanthanide complex itself can behave as a SMM.[4a,b] Since then, the magnetic properties of lanthanide complexes have been investigated extensively,[4c,d] and now Dy^{III} complexes with strong Ising type magnetic anisotropy are considered to be among the most promising compounds for the development of SMMs with high blocking temperatures and large relaxation barriers.[5] For mononuclear Dy^{III} complexes, SIM (Single Ion Magnet) behavior is attributed to the crystal-field splitting of the lowest J multiplet. For polynuclear Dy^{III} clusters, the SMM properties are still strongly determined by the SIM behavior, although they can be significantly affected by the weak f−f exchange coupling. Some of the polynuclear Dy^{III} complexes showed the sharp increase of $\chi_M T$ at the low temperature region due to the presence of intramolecular ferromagnetic Dy^{III}−Dy^{III} interaction and exhibited a remarkably large energy barrier in their SMM nature.[6] However, the crystal-field splitting, the complexity of the electronic levels pattern determining the magnetic anisotropy easy-axes, and the f−f exchange coupling in polynuclear systems make difficult the rationalization of the SMM behavior and, therefore, the magnetic properties of lanthanide complexes are still characterized by many unclear aspects.

Recently, several carbonato-bridged lanthanide clusters were studied for their SMM properties.[7] Previously, we reported the first example of atmospheric CO_2 fixation by transition metal−lanthanide (3d−4f) complex.[8] The resultant tetranuclear $Ni^{II}_2Ln^{III}_2$ complexes (Ln^{III} = Gd^{III}, Tb^{III}, Dy^{III}) are formulated as $[(\mu_4\text{-}CO_3)_2\{Ni^{II}L^1(MeOH)Ln^{III}(NO_3)\}_2]$ (L^1 = *N*,*N*′-bis(3-methoxy-2-oxybenzylidene)-1,3-propanediaminato), and their structures are described as two di-μ-phenoxo-bridged $\{Ni^{II}L^1(MeOH)Ln^{III}(NO_3)\}$ binuclear units bridged by two carbonato CO_3^{2-} ions. The $Ni^{II}_2Tb^{III}_2$ and $Ni^{II}_2Dy^{III}_2$ complexes showed an out-of-phase signal in alternating current (ac) susceptibility measurements, indicative of slow relaxation of magnetization of SMM. As the molecular system involves high-spin (S = 1) Ni^{II} ions with significant zero-field splitting (ZFS), strongly anisotropic Ln^{III} ions and Ni^{II}−Ln^{III} and Ln^{III}−Ln^{III} exchange couplings, it is difficult to separate these effects and to rationalize the magnetic behavior.

In this study, a paramagnetic Ni^{II} ion with ZFS is substituted for a diamagnetic Zn^{II} ion and two series of carbonato-bridged $Zn^{II}_2Ln^{III}_2$ complexes are synthesized. The first series of $Zn^{II}_2Ln^{III}_2$ complexes with the formula $[(\mu_4\text{-}CO_3)_2\{Zn^{II}L^1Ln^{III}(NO_3)\}_2]$ are abbreviated as **ZnGd1**, **ZnTb1**, and **ZnDy1** and the second series of $Zn^{II}_2Ln^{III}_2$ complexes with the formula $[(\mu_4\text{-}CO_3)_2\{Zn^{II}L^2Ln^{III}(NO_3)\}_2]$ (L^2 = *N*,*N*′-bis(3-ethoxy-2-oxybenzylidene)-1,3-propanediaminato) are abbreviated as **ZnGd2**, **ZnTb2**, and **ZnDy2**. Their crystal structures are determined, and their magnetic properties are measured. Because the Zn^{II} ion with a d^{10} electronic configuration is diamagnetic, the magnetic model structure of the $Zn^{II}_2Ln^{III}_2$ complexes is drawn as Scheme 1 on the basis of the molecular structure. The magnetic properties of the $Zn^{II}_2Ln^{III}_2$ complexes depend on the energy level pattern resulting from the Stark splitting of the ground state of the Ln^{III} ions perturbed by the Ln^{III}−Ln^{III} magnetic interaction. The magnetic properties of

Scheme 1. Spin Structure Based on Structure of Dicarbonato-Bridged $Zn^{II}_2Ln^{III}_2$ Complex

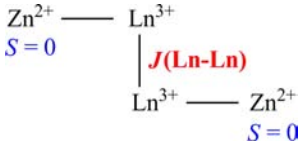

$Zn^{II}_2Ln^{III}_2$ complexes were therefore analyzed by a Hamiltonian including the crystal-field effect on the Ln^{III} ions and the Ln^{III}−Ln^{III} magnetic interaction. The Gd^{III} and Tb^{III} complexes of both series (**ZnGd1**, **ZnGd2**) and (**ZnTb1**, **ZnTb2**) show ferromagnetic Ln^{III}−Ln^{III} interactions. Though luminescence spectra of **ZnDy1** and **ZnDy2** were not observed, those of **ZnTb1** and **ZnTb2** were observed and the fine structure assignable to the $^5D_4 \rightarrow {}^7F_6$ transition has been correlated to the energy diagram from the magnetic analysis. As to the Dy^{III} complexes, **ZnDy1** shows a Dy^{III}−Dy^{III} ferromagnetic interaction, whereas **ZnDy2** shows an antiferromagnetic interaction. Alternating current (ac) susceptibility measurements demonstrated that the $Zn^{II}_2Ln^{III}_2$ complexes (Ln^{III} = Tb^{III}, Dy^{III}) showed out-of-phase signal with frequency-dependence, indicative of SMM. We report here the synthesis, structures, luminescent, and magnetic properties of these $Zn^{II}_2Ln^{III}_2$ complexes.

EXPERIMENTAL SECTION

Materials. All reagents and solvents, obtained from Tokyo Kasei Co. and Wako Pure Chemical Industries, in the syntheses were of reagent grade, and they were used without further purification. All reactions were carried out under ambient atmosphere.

Component Zn^{II} Complexes. Tetradentate N_2O_2 Schiff-base ligands H_2L^1 and H_2L^2 were synthesized by the 1:2 condensation reactions of 1,3-propanediamine and either 3-methoxysalicylaldehyde or 3-ethoxysalicylaldehyde in ethanol according to the conventional method for the Schiff-base ligands. The component Zn^{II} complexes $[Zn^{II}L^1(H_2O)_2]\cdot 3.5H_2O$ and $[Zn^{II}L^2(H_2O)_2]\cdot 2H_2O$ were synthesized by mixing zinc(II) acetate dihydrate and either H_2L^1 or H_2L^2 in a 1:1 mol ratio in ethanol, according to the method reported in the literature.[9]

$[(\mu_4\text{-}CO_3)_2\{Zn^{II}L^1Gd^{III}(NO_3)\}_2]\cdot$acetone$\cdot 2H_2O$ (ZnGd1). To a solution of $Gd^{III}(NO_3)_3\cdot 6H_2O$ (135 g, 0.3 mmol) in 10 mL of MeOH was added triethylamine (33 mg, 0.3 mmol) at ambient temperature. To the resultant mixture was added a solution of $[Zn^{II}L^1(H_2O)_2]\cdot 3.5H_2O$ (122 mg, 0.3 mmol) in 20 mL of MeOH and 10 mL of acetone at room temperature. The color of the mixed solution changed from yellow to colorless in 10 min. The mixture was filtered, and the filtrate was left to stand under ambient atmosphere for a few days, during which time small colorless crystals precipitated. The crystals were collected by suction filtration and dried in vacuo. The crystals are effluorescent. Yield: 123 mg (30%). $[(\mu_4\text{-}CO_3)_2\{Zn^{II}L^1Gd^{III}(NO_3)\}_2]\cdot$acetone$\cdot 2H_2O$. Anal. Calcd for $(C_{20}H_{20}N_3O_{10}ZnGd)_2\cdot$acetone$\cdot 2H_2O$: C, 35.27; H, 3.44; N, 5.74%. Found: C, 35.31; H, 3.54; N, 5.67%. IR (KBr, cm^{-1}): ν(C=N) 1625, $\nu(NO_3^-)$ 1384, $\nu(CO_3)$ 1475, 1440, 740. TGA: 3.6% weight loss corresponding to three H_2O molecules (3.8%) was observed in the temperature region lower than 120 °C on the heating process, suggesting that acetone in the sample for the elemental analysis was substituted for H_2O for the TGA sample.

$[(\mu_4\text{-}CO_3)_2\{Zn^{II}L^1Tb^{III}(NO_3)\}_2]\cdot$acetone$\cdot H_2O$ (ZnTb1). **ZnTb1** was synthesized in a similar way to **ZnGd1**, using $Tb^{III}(NO_3)_3\cdot 6H_2O$ instead of $Gd^{III}(NO_3)_3\cdot 6H_2O$. Colorless crystals. Yield: 122 mg (30%). Anal. Calcd for $(C_{20}H_{20}N_3O_{10}ZnTb)_2\cdot$acetone$\cdot H_2O$: C; 35.63, H; 3.38, N; 5.80%. Found: C; 35.68, H; 3.63, N; 5.66%. IR (KBr, cm^{-1}): ν(C=N) 1633, $\nu(NO_3^-)$ 1384, $\nu(CO_3)$ 1471, 1440, 738. TGA: 2.6% weight loss corresponding to two H_2O molecules (2.6%) was observed in the temperature region lower than 140 °C on the heating process, suggesting that acetone was substituted for H_2O for the TGA sample.

dx.doi.org/10.1021/ic4022273 | Inorg. Chem. 2013, 52, 12828−12841

Table 1. X-ray Crystallographic Data for $Zn^{II}_2Ln^{III}_2$ Complexes $[(\mu_4\text{-}CO_3)_2\{Zn^{II}L^1Ln^{III}(NO_3)\}_2]\cdot 2$acetone, ZnGd1, ZnTb1, and ZnDy1

formula	$C_{46}H_{52}N_6O_{22}Gd_2Zn_2$	$C_{46}H_{52}N_6O_{22}Tb_2Zn_2$	$C_{46}H_{52}N_6O_{22}Dy_2Zn_2$
fw	1486.20	1489.56	1496.70
crystal system	monoclinic	monoclinic	monoclinic
space group	$P2_1/c$ (No. 14)	$P2_1/c$ (No. 14)	$P2_1/c$ (No. 14)
a, Å	11.6854(3)	11.674(1)	11.6705(4)
b, Å	10.4936(4)	10.5066(8)	10.4618(5)
c, Å	20.9998(5)	20.976 (2)	20.9683(6)
β, deg	90.1120(7)	90.250(3)	90.032(1)
V, Å^3	2575.0(1)	2572.8(4)	2560.1(2)
Z	2	2	2
T, K	150	150	150
D_{calcd}, g cm^{-3}	1.917	1.923	1.941
μ, cm^{-1}	35.577	37.192	39.040
R, wR	0.0401, 0.1155	0.0545, 0.1461	0.0348, 0.1033

$[(\mu_4\text{-}CO_3)_2\{Zn^{II}L^1Dy^{III}(NO_3)\}_2]\cdot 0.5$acetone$\cdot 3H_2O$ (ZnDy1). **ZnDy1** was synthesized in a similar way to **ZnGd1**, using $Dy^{III}(NO_3)_3\cdot 6H_2O$ instead of $Gd^{III}(NO_3)_3\cdot 6H_2O$. Colorless crystals. Yield: 124 mg (30%). Anal. Calcd for $(C_{20}H_{20}N_3O_{10}ZnDy)_2\cdot 0.5$acetone$\cdot 3H_2O$: C; 34.06, H; 3.38, N; 5.74%. Found: C; 34.01, H; 3.21, N; 5.86%. IR (KBr, cm^{-1}): ν(C═N) 1633, $\nu(NO_3^-)$ 1384, $\nu(CO_3)$ 1471, 1440, 740. TGA: 3.4% weight loss corresponding to three H_2O molecules (3.7%) was observed in the temperature region lower than 170 °C on the heating process, suggesting that 0.5 acetone was eliminated for the TGA sample.

$[(\mu_4\text{-}CO_3)_2\{Zn^{II}L^2Gd^{III}(NO_3)\}_2]\cdot 2.5H_2O$ (ZnGd2). To a solution of $Gd^{III}(NO_3)_3\cdot 6H_2O$ (135 mg, 0.3 mmol) in 10 mL of MeOH was added triethylamine (33 mg, 0.3 mmol) at ambient temperature. To the resultant mixture was added a solution of $[Zn^{II}L^2(H_2O)]\cdot 2H_2O$ (135 mg, 0.3 mmol) in 20 mL of MeOH and 10 mL of acetone at room temperature. The color of the mixed solution changed from yellow to colorless in 10 min. The mixture was filtered, and the filtrate was left to stand for a few days under ambient atmosphere, during which time small colorless brick crystals precipitated. The crystals were collected by suction filtration and dried in vacuo. The crystals are effluorescent. Yield: 122 mg (55%). $[(\mu_4\text{-}CO_3)_2\{Zn^{II}L^2Gd^{III}(NO_3)\}_2]\cdot 2.5H_2O$, Anal. Calcd for $(C_{22}H_{24}N_3O_{10}ZnGd)_2\cdot 2.5H_2O$: C, 35.92; H, 3.63; N, 5.71%. Found: C, 35.93; H, 3.62; N, 5.71%. IR (KBr, cm^{-1}): ν(C═N) 1625, $\nu(NO_3^-)$ 1384, $\nu(CO_3^{2-})$ 1463, 732. TGA: 3.04% is the calculated value of 2.5 water molecules per tetramer; 3.20% weight loss was observed in the temperature region below 130 °C.

$[(\mu_4\text{-}CO_3)_2\{Zn^{II}L^2Tb^{III}(NO_3)\}_2]\cdot 2.5H_2O$ (ZnTb2). **ZnTb2** was synthesized in a similar way to **ZnGd2**, using $Tb^{III}(NO_3)_3\cdot 6H_2O$ instead of $Gd^{III}(NO_3)_3\cdot 6H_2O$. Colorless brick crystals. Yield: 115 mg (52%). Anal. Calcd for $(C_{22}H_{24}N_3O_{10}ZnTb)_2\cdot 2.5H_2O$: C; 35.84, H; 3.62, N; 5.70%. Found: C; 35.75, H; 3.63, N; 5.74%. IR (KBr, cm^{-1}): ν(C═N) 1625, $\nu(NO_3^-)$ 1384, $\nu(CO_3^{2-})$ 1463, 734. TGA: 3.04% is the calculated value of 2.5 water molecules per tetrameric unit; 3.20% weight loss was observed in the temperature region lower than 130 °C.

$[(\mu_4\text{-}CO_3)_2\{Zn^{II}L^2Dy^{III}(NO_3)\}_2]\cdot 2.5H_2O$ (ZnDy2). **ZnDy2** was synthesized in a similar way to **ZnGd2**, using $Dy^{III}(NO_3)_3\cdot 6H_2O$ instead of $Gd^{III}(NO_3)_3\cdot 6H_2O$. Colorless brick crystals. Yield: 120 mg (54%). Anal. Calcd for $(C_{22}H_{24}N_3O_{10}ZnDy)_2\cdot 2.5H_2O$: C; 35.67, H; 3.61, N; 5.67%. Found: C; 35.69, H; 3.58, N; 5.77%. IR (KBr, cm^{-1}): ν(C═N) 1625, $\nu(NO_3^-)$ 1384, $\nu(CO_3^{2-})$ 1463, 734. TGA: 3.03% is the calculated value to 2.5 water molecules per tetrameric unit; 3.10% weight loss was observed on the heating process.

Physical Measurements. Elemental analyses (C, H, and N) were carried out at the Center for Instrumental Analysis of Kumamoto University. Infrared spectra were recorded at room temperature using a JEOL JIR-6500W spectrometer with samples in KBr disks. Thermogravimetric analyses (TGA) were carried out on a TG/DTA6200 (SII Nano Technology Inc.) instrument at a 5 K min^{-1} heating rate using a ca. 5 mg sample. Excitation and emission spectra in the polycrystalline solid state were measured on a HITACHI F-7000 fluorescence spectrophotometer according to the procedure reported previously.[10] Temperature-dependent magnetic susceptibilities in the temperature range 1.9−300 K under an external magnetic field of 0.1 T and field-dependent magnetization measurements in an applied magnetic field from 0 to 5 T at 1.9 K were measured with an MPMS XL5 SQUID susceptometer (Quantum Design, Inc.). Microcrystalline samples consisting of Tb^{III} and Dy^{III} ions showed apparent reorientation in the applied magnetic field of 0.1 T. All samples dispersed in liquid paraffin to avoid orientation in the field. The calibrations were performed with palladium. Corrections for diamagnetism were applied using Pascal's constants.[11] The ac magnetic susceptibility was measured on a Quantum Design PPMS alternating current/direct current (ac/dc) magnetometer in a temperature range down to 2.0 K under 0 and 1000 Oe dc fields.

X-ray Data Collection and Structure Determination. The two series of complexes (**ZnGd1**, **ZnTb1**, and **ZnDy1**) and (**ZnGd2**, **ZnTb2**, and **ZnDy2**) were crystallized as small prismatic crystals from the solution of methanol/acetone. The crystals were effluorescent, and the crystal used for the X-ray diffraction study was picked up from the reaction vessel, and coated by epoxy resin. The X-ray data collections were collected at 150 K on a Rigaku Rapid imaging plate diffractometer with graphite monochromated Mo Kα radiation (λ = 0.710 69 Å). The structures were solved by direct methods and refined on F^2 by a full-matrix least-squares procedure.[12] All calculations were performed using the CrystalStructure crystallographic software package.[13]

RESULTS AND DISCUSSION

Synthesis and Characterization of $Zn^{II}_2Ln^{III}_2$ Complexes (Ln = Gd, Tb, Dy). The first series of $Zn^{II}_2Ln^{III}_2$ complexes (**ZnGd1**, **ZnTb1**, and **ZnDy1**) with H_2L^1 = *N*,*N*′-bis(3-methoxy-2-oxybenzylidene)-1,3-propanediamine were synthesized by mixing $[Zn^{II}L^1(H_2O)_2]\cdot 3.5H_2O$, $Ln^{III}(NO_3)_3\cdot 6H_2O$, and triethylamine with a 1:1:1 molar ratio in a mixed solvent of methanol and acetone at room temperature under ambient atmosphere. While the mixed solution was allowed to stand for several days, atmospheric CO_2 fixation occurred and colorless crystals precipitated. X-ray analyses showed the chemical formula of $[(\mu_4\text{-}CO_3)_2\{Zn^{II}L^1Ln^{III}(NO_3)\}_2]\cdot 2$acetone, where the compounds contain two acetone molecules per $Zn^{II}_2Ln^{III}_2$ as the crystal solvent. The crystals are effluorescent. The elemental analyses of the effluorescent sample agreed with the chemical formula of $[(\mu_4\text{-}CO_3)_2\{Zn^{II}L^1Ln^{III}(NO_3)\}_2]\cdot x$acetone$\cdot yH_2O$, and the content of acetone decreases gradually and is substituted for water molecules in the open atmosphere. These complexes exhibit IR absorption bands assigned to carbonate ion.[14] The asymmetric ν_3 stretching vibrations of carbonate and the in-plane ν_4 deformation of $\nu(CO_3)$ are clearly seen at 1440 and 740 cm^{-1}, respectively. The IR spectra showed a characteristic band at 1625 cm^{-1} assignable to C═N stretching vibration of Schiff-base

dx.doi.org/10.1021/ic4022273 | Inorg. Chem. 2013, 52, 12828−12841

ligand. The strong absorptions at 1384 cm^{-1} are due to the presence of the nitrate groups.

The second series of $Zn^{II}_2Ln^{III}_2$ complexes (**ZnGd2**, **ZnTb2**, and **ZnDy2**) were synthesized in a similar way of **ZnGd1**, **ZnTb1**, and **ZnDy1** by the use of $[Zn^{II}L^2(H_2O)_2]\cdot 2H_2O$ instead of $[Zn^{II}L^1(H_2O)_2]\cdot 3.5H_2O$. The X-ray analyses showed the formula of $[(\mu_4\text{-}CO_3)_2\{Zn^{II}L^2Ln^{III}(NO_3)\}_2]\cdot 2MeOH\cdot H_2O$, where the compounds contain two methanol and one water per $Zn^{II}_2Ln^{III}_2$ as the crystal solvent. The crystals are effluorescent. The elemental analyses of the effluorescent sample agreed with the chemical formula of $[(\mu_4\text{-}CO_3)_2\{Zn^{II}L^1Ln^{III}(NO_3)\}_2]\cdot 2.5H_2O$ for **ZnGd2**, **ZnTb2**, and **ZnDy2**, indicating that two methanol molecules are substituted for 2.5 water molecules in the open atmosphere. The TGA analyses detected the weight loss corresponding to $2.5H_2O$. These complexes exhibit carbonato-related IR absorption bands, a characteristic band at 1625 cm^{-1} assignable to C═N stretching vibration of Schiff-base ligand, and strong absorption at 1384 cm^{-1} due to nitrate ion.

Molecular Structures of $Zn^{II}_2Ln^{III}_2$ Complexes of L^1. The crystallographic data of the $Zn^{II}_2Ln^{III}_2$ complexes of L^1 (**ZnGd1**, **ZnTb1**, and **ZnDy1**) are listed in Table 1. The coordination bond distances and the relevant angles are listed in Table 2. All

Table 2. Coordination Bond Distances (Å), $Ln^{III}\cdots Ln^{III}$ Distance (Å), and $Ln^{III}\cdots M^{II}$ Distances for ZnGd1, ZnTb1, and ZnDy1

	ZnGd1	ZnTb1	ZnDy1
Ln−O1	2.518(3)	2.518(5)	2.507(4)
Ln−O2	2.332(3)	2.312(5)	2.302(4)
Ln−O3	2.357(3)	2.332(5)	2.336(4)
Ln−O4	2.501(4)	2.494(5)	2.483(4)
Ln−O6	2.394(3)	2.376(5)	2.361(4)
Ln−O6*	2.364(3)	2.345(5)	2.331(4)
Ln−O7*	2.422(3)	2.400(5)	2.392(4)
Ln−O8	2.535(4)	2.529(5)	2.511(4)
Ln−O9	2.501(4)	2.484(5)	2.469(4)
Zn−O2	2.074(3)	2.073(4)	2.083(3)
Zn−O3	2.064(4)	2.069(5)	2.060(4)
Zn−O5	1.997(4)	2.001(5)	2.005(4)
Zn−N1	2.065(4)	2.062(6)	2.065(5)
Zn−N2	2.076(4)	2.079(6)	2.073(5)
Ln···Zn	3.4666(5)	3.4573(8)	3.4516(5)
Ln···Ln*	4.0454(3)	4.0206(5)	3.9912(3)
Zn −O2−Ln	103.6(1)	104.0(2)	103.7(1)
Zn −O3−Ln	103.1(1)	103.4(2)	103.3(1)
Ln−O6−Ln*	116.5(1)	116.8(2)	116.6(2)

three $Zn^{II}_2Ln^{III}_2$ complexes crystallized in a same monoclinic space group $P2_1/n$ (No. 14) with the similar cell dimensions involving two acetone molecules per $Zn^{II}_2Ln^{III}_2$ cluster as the crystal solvent, indicating that they have an isomorphous structure to each other.

The structure of **ZnDy1** is described in detail as the representative example and is shown in Figure 1a,b. The complex has a tetranuclear $Zn^{II}_2Dy^{III}_2$ structure that can be described as two di-μ-phenoxo-bridged $\{Zn^{II}L^1Ln^{III}(NO_3)\}$ binuclear units bridged by two carbonato CO_3^{2-} ions. This tetranuclear structure is essentially the same as that of the previously reported $Ni^{II}_2Ln^{III}_2$ complexes.[8] In the $(\mu_4\text{-}CO_3)_2Zn^{II}_2Dy^{III}_2$ tetranuclear structure, one carbonate ion (O5, O6, O7, or C20) bridges the Zn^{II} and Dy^{III} ions of a binuclear unit with Zn−O5 = 2.005(4) and Dy−O6 = 2.361(4) Å, and further coordinates to the Dy^{III} ion of the adjacent binuclear unit (Dy*) as a chelate ligand with Dy*−O6 = 2.331(4) Å and Dy*−O7 = 2.392(4) Å (an asterisk indicates a symmetry operation of inversion). One carbonato ion thus acts as a tetradentate ligand and links one Zn and two Dy ions. Dy···Dy* distance is 3.9912(3) Å.

The Dy^{III} ion is coordinated by the four oxygen atoms of two phenoxo (Dy−O2 = 2.302(4), Dy−O3 = 2.336(4) Å) and two methoxy oxygen atoms (Dy−O1 = 2.507(4) Å, Dy−O4 = 2.483(4) Å) of $(Zn^{II}L^1)$, two oxygen atoms of NO_3^- ion acting as a chelate ligand with Dy−O8 = 2.511(4) Å and Dy−O9 = 2.469(4) Å, two oxygen atoms of a carbonato ion with Dy−O6* = 2.331(4) Å and Dy−O7* = 2.392(4) Å, and one oxygen atom of another carbonato ion with Dy−O6 = 2.361(4) Å; therefore, a coordination number of nine is attained. The Zn^{II} ion assumes a square pyramidal coordination geometry with N_2O_2 donor atoms of L^1 at the equatorial plane and one oxygen atom O5 of CO_3^{2-} at the axial position with Zn−O5 = 2.005(4) Å. The Zn atom deviated from the equatorial coordination plane (N_2O_2 plane) by 0.42 Å toward the axial coordination atom O5. The dihedral angle between the planes of ZnO2O3 and DyO2O3 in the bridging core of ZnO_2Dy is 25.4°, whose value is larger than 14.2 and 11.5°, those for the corresponding NiO_2Dy complexes with six-coordinated geometry around Ni^{II} ion.[8] The plane of NO_3^- laid on the direction of one of Dy−O(methoxy) bonds, Dy−O1.

There is no intermolecular hydrogen bonding between the adjacent tetramers and between the tetramer and acetone, demonstrating that **ZnDy1** can be described as an isolated tetranuclear $Zn^{II}_2Dy^{III}_2$ molecule (Figure S1, Supporting Information).

Molecular Structures of $Zn^{II}_2Ln^{III}_2$ Complexes of L^2. The crystallographic data of the $Zn^{II}_2Ln^{III}_2$ complexes of L^2 (**ZnGd2**, **ZnTb2**, and **ZnDy2**) are listed in Table 3. The coordination bond distances and the relevant angles are listed in Table 4. All three $Zn^{II}_2Ln^{III}_2$ complexes crystallized in triclinic space group $P\bar{1}$ (No. 2) with the similar cell dimensions, indicating that they have an isomorphous structure. The unit cell consists of two tetranuclear $Zn^{II}_2Ln^{III}_2$ complexes; tetramer A and tetramer B, where each tetramer has an inversion center, and tetramers A and B have a similar structure to those of **ZnLn1** and the $Ni^{II}_2Ln^{III}_2$ complexes. The structure of **ZnDy2** is described as the representative example. Tetramer A and tetramer B have a similar structure except for one of two ethoxy groups of tetramer B, which suffers from disorder. The molecular structure of **ZnDy2** is shown in Figure 2a,b. The tetranuclear $Zn^{II}_2Dy^{III}_2$ structure is described as that two di-μ-phenoxo-bridged $\{Zn^{II}L^2Ln^{III}(NO_3)\}$ binuclear units bridged by two carbonato CO_3^{2-} ions, in which one carbonato ion acts as a tetradentate ligand and links one Zn and two Dy ions. The Dy^{III} ion is coordinated by the four oxygen atoms of two phenoxo (Dy1−O2 = 2.350(6) Å, Dy1−O3 = 2.313(6) Å) and two ethoxy oxygen atoms (Dy1−O1 = 2.512(6) Å, Dy1−O4 =2.512(6) Å) of $(Zn^{II}L^2)$, two oxygen atoms of NO_3^- ion acting as a chelate ligand with Dy1−O8 = 2.475(6) Å and Dy1−O9 = 2.506(6) Å, two oxygen atoms of a carbonato ion with Dy1−O6* = 2.333(6) Å and Dy1−O7* = 2.401(6) Å, and one oxygen atom of another carbonato ion with Dy1−O6 = 2.390(5) Å; therefore, a coordination number of nine is attained. The Zn^{II} ion assumes a square pyramidal coordination geometry with N_2O_2 donor atoms of L^2 at the equatorial plane and one oxygen atom O5 of CO_3^{2-} at the axial position with Zn1−O5 = 2.017(6) Å for

dx.doi.org/10.1021/ic4022273 | Inorg. Chem. 2013, 52, 12828−12841

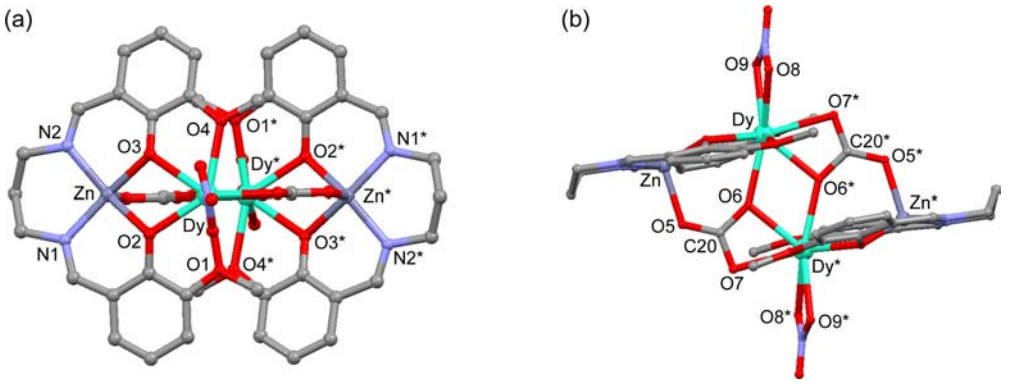

Figure 1. Molecular structures of the tetranuclear $Zn^{II}_2Dy^{III}_2$ complex (**ZnDy1**) with the selected atom numbering scheme. The tetranuclear $Zn^{II}_2Dy^{III}_2$ molecule has an inversion center, and the hydrogen atoms are omitted for clarity. (a) Perspective view of **ZnDy1** projected on the N_2O_2 equatorial coordination planes. (b) Side view showing the $(\mu_4\text{-}CO_3)_2\{Zn^{II}_2Dy^{III}_2\}$ structure and the coordination of a nitrato ion as a chelate ligand to the Dy^{III} ion.

Table 3. X-ray Crystallographic Data for $Zn^{II}_2Ln^{III}_2$ Complexes $[(\mu_4\text{-}CO_3)_2\{Zn^{II}L^2Ln^{III}(NO_3)\}_2]\cdot 2MeOH\cdot H_2O$, ZnGd2, ZnTb2, and ZnDy2

formula	$C_{46}H_{57}N_6O_{22.5}Gd_2Zn_2$	$C_{46}H_{57}N_6O_{22.5}Tb_2Zn_2$	$C_{46}H_{57}N_6O_{22.5}Dy_2Zn_2$
fw	1499.24	1502.59	1509.74
crystal system	triclinic	triclinic	triclinic
space group	$P\bar{1}$ (No. 2)	$P\bar{1}$ (No. 2)	$P\bar{1}$ (No. 2)
a, Å	10.346(1)	10.3655(8)	10.3666(4)
b, Å	13.746(2)	13.7310(8)	13.7360(5)
c, Å	19.048(2)	19.089(1)	18.9393(8)
a, deg	83.894(4)	83.796(2)	83.750(1)
β, deg	80.980(3)	80.553(2)	80.930(1)
γ, deg	83.788(4)	83.200(2)	83.777(1)
V, Å^3	2648.6(5)	2650.4(3)	2635.9(2)
Z	2	2	2
T, K	150	150	150
D_{calcd}, g cm^{-3}	1.880	1.883	1.902
μ, cm^{-1}	34.60	36.12	37.94
R, w*R*	0.0911, 0.2227	0.0664, 0.1478	0.0494, 0.1066

Table 4. Coordination Bond Distances (Å), $Ln^{III}\cdots Ln^{III}$ Distance (Å), and $Ln^{III}\cdots M^{II}$ Distances (Å) for ZnGd2, ZnTb2, and ZnDy2

tetramer A				tetramer B			
tetramer A	**ZnGd2**	**ZnTb2**	**ZnDy2**		**ZnGd2**	**ZnTb2**	**ZnDy2**
Ln1−O1	2.498(10)	2.513(8)	2.512(6)	Ln2−O11	2.558(11)	2.541(8)	2.506(6)
Ln1−O2	2.375(13)	2.336(9)	2.350(6)	Ln2−O12	2.299(14)	2.329(9)	2.305(6)
Ln1−O3	2.328(13)	2.336(8)	2.313(6)	Ln−O13	2.353(12)	2.325(10)	2.338(7)
Ln1−O4	2.518(12)	2.532(8)	2.512(6)	Ln2−O14	2.494(1)	2.494(9)	2.516(6)
Ln1−O6	2.406(10)	2.396(8)	2.390(5)	Ln2−O16	2.339(11)	2.381(9)	2.372(6)
Ln1−O6*	2.37(1)	2.366(8)	2.333(6)	Ln2−O16*	2.34(1)	2.36(1)	2.329(6)
Ln1−O7*	2.44(1)	2.43(1)	2.401(6)	Ln2−O17*	2.43(1)	2.42(1)	2.403(7)
Ln1−O8	2.518(11)	2.506 (8)	2.475(6)	Ln2−O18	2.548(11)	2.539(9)	2.505(6)
Ln1−O9	2.542(11)	2.528(8)	2.506(6)	Ln2−O19	2.471(12)	2.465(9)	2.450(6)
Zn1−O2	2.044(13)	2.058(8)	2.051(6)	Zn2−O12	2.066(13)	2.071(10)	2.085(6)
Zn1−O3	2.070(12)	2.086(9)	2.095(6)	Zn2−O13	2.072(13)	2.073(9)	2.073(6)
Zn1−O5	1.996(10)	2.014(8)	2.017(5)	Zn2−O15	1.982(10)	2.016(8)	2.011(6)
Zn1−N1	2.066(15)	2.065(12)	2.053(8)	Zn2−N4	2.033(18)	2.068(11)	2.053(10)
Zn1−N2	2.082(16)	2.061(11)	2.084(8)	Zn2−N5	2.091(16)	2.072(13)	2.030(8)
Ln1···Zn1	3.489(2)	3.488(2)	3.472(1)	Ln2···Zn2	3.481(2)	3.484(2)	3.462(1)
Ln1···Ln1*	4.075(1)	4.0583(8)	4.0298(5)	Ln2···Ln2*	4.050(1)	4.0419(8)	4.0069(5)
Zn1−O2−Ln1	104.1(5)	104.9(3)	104.0(3)	Zn2−O12−Ln2	105.6(6)	104.6(4)	103.8(3)
Zn1−O3−Ln1	104.9(5)	104.0(3)	103.8(3)	Zn2−O13−Ln2	103.6(5)	104.6(4)	103.2(3)
Ln1−O6−Ln1*	116.9(4)	116.9(3)	117.1(2)	Ln2−O16−Ln2*	116.8(4)	117.1(4)	116.8(3)

tetramer A and Zn2−O15 = 2.012(5) Å for tetramer B. The Zn atoms of tetramers A and B deviate from the equatorial coordination plane by 0.45 and 0.47 Å toward the axial coordination atom O5 andO15, respectively. The two Zn−O−

dx.doi.org/10.1021/ic4022273 | *Inorg. Chem.* 2013, 52, 12828−12841

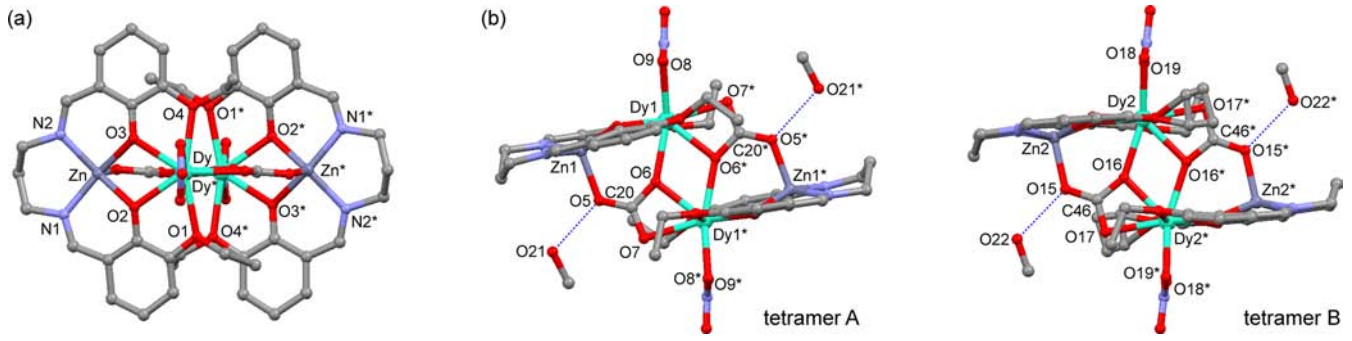

Figure 2. Molecular structure of the tetranuclear $Zn^{II}_2Dy^{III}_2$ complex (**ZnDy2**) with the selected atom numbering schemes. The tetranuclear $Zn^{II}_2Dy^{III}_2$ molecule has an inversion center, and the hydrogen atoms are omitted for clarity. (a) Perspective view of tetramer A of **ZnDy2** projected on the N_2O_2 equatorial coordination planes. (b) Side view of tetramers A and B showing the $(\mu_4\text{-}CO_3)_2\{Zn^{II}_2Dy^{III}_2\}$ structure, a nitrato ion as a chelate ligand to a Dy^{III} ion, and hydrogen bond between methanol and CO_3^{2-}. One ethoxy group of tetramer B is suffers from disorder.

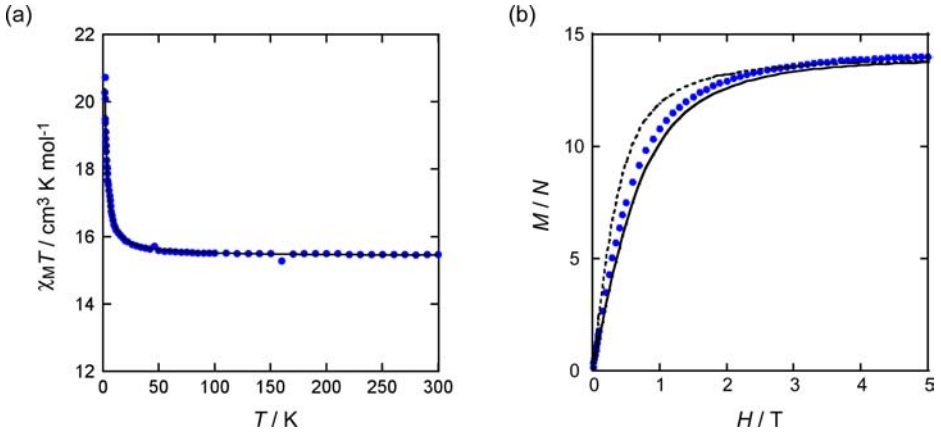

Figure 3. (a) Plots of $\chi_M T$ per $Zn^{II}_2Gd^{III}_2$ vs T for **ZnGd1**. The solid line represents the theoretical curve with the best-fit parameters of $g_{Gd} = 1.98$ and $J(\text{Gd}-\text{Gd}) = +0.042\ \text{cm}^{-1}$. (b) Field dependence of the magnetization at 1.9 K for **ZnGd1**, as plots of $M/N\beta$ vs H. The solid and dotted lines represent the theoretical curves of $M = Ng_{Gd}\beta SB_S(y) \times 2$ with $g_{Gd} = 1.98$ and $S = 7/2$ and $M = Ng_{Gd}\beta SB_S(y)$ with $g_{Gd} = 1.98$ and $S = 7$, respectively. For **ZnGd2**, see Figure S3, Supporting Information.

Dy bridging angles in the ZnO_2Dy unit are 104.0(3) and 103.8(3)°. The dihedral angle between the planes of ZnO2O3 and DyO2O3 in the bridging core of ZnO_2Dy is 25.6°. The plane of NO_3^- is perpendicular to the direction of $Zn^{II} \rightarrow Dy^{III}$.

Oxygen atom O5 of CO_3^{2-} at the axial position for tetramer A participates to the formation of hydrogen bond to a methanol with O5···O21 = 2.760 Å. For tetramer B, O15 is similarly hydrogen bonded to O22 with O5···O22 = 2.743 Å. There are no other intermolecular short contacts between the adjacent tetramers and between the tetramer and methanol (Figure S2, Supporting Information).

Magnetic Properties of $Zn^{II}_2Gd^{III}_2$ Complexes. The temperature dependences of dc magnetic susceptibilities were measured on powdered samples dispersed in paraffin grease in the temperature range of 1.9–300 K under a direct current (dc) field of 0.1 T. The field dependences of the magnetization at 1.9 K were measured from 0 to 5 T. The two $Zn^{II}_2Gd^{III}_2$ complexes, **ZnGd1** and **ZnGd2**, exhibit a similar magnetic behavior. Figure 3a shows the temperature dependences of the magnetic susceptibilities of **ZnGd1**, as plots of $\chi_M T$ vs T, where χ_M is the molar magnetic susceptibility per tetranuclear $Zn^{II}_2Gd^{III}_2$ molecule and T is the absolute temperature. The magnetic susceptibilities follow the Curie–Weiss equation defined by $1/\chi_M = C(T - \theta)$, with $\theta = +0.52$ and +0.45 K for **ZnGd1** and **ZnGd2**, respectively, indicating the operation of weak ferromagnetic interactions. The room temperature $\chi_M T$ values of **ZnGd1** and **ZnGd2** are 15.468 and 16.024 $\text{cm}^3\ \text{K}\ \text{mol}^{-1}$, respectively, whose values are close to the value of 15.75 $\text{cm}^3\ \text{K}\ \text{mol}^{-1}$ expected for two diamagnetic Zn^{II} ion ($3d^{10}$, $S = 0$) and two noninteracting Gd^{III} ($4f^7$, $J = 7/2$, $L = 0$, $S = 7/2$, $^8S_{7/2}$) ions assuming $g_{Gd} = 2.00$. When the temperature is lowered from 300 to 1.9 K, the $\chi_M T$ values of both complexes remain essentially constant until ca. 30 K and then steadily increase to 20.72 and 19.47 $\text{cm}^3\ \text{K}\ \text{mol}^{-1}$ at 1.9 K for **ZnGd1** and **ZnGd2**, respectively. The increase of $\chi_M T$ values in the lower temperature region indicates a weak intramolecular Gd^{III}–Gd^{III} ferromagnetic interaction. Because the Zn^{II} ion is diamagnetic and Gd^{III} has no contribution from orbital angular momentum, the magnetic behavior has been interpreted by an isotropic spin Hamiltonian of $\mathbf{H} = \beta g_{Gd}(\hat{\mathbf{S}}_{Gd1} + \hat{\mathbf{S}}_{Gd2})\cdot H - 2J(\text{Gd}-\text{Gd})\hat{\mathbf{S}}_{Gd1}\cdot\hat{\mathbf{S}}_{Gd2}$ for the spin structure in Scheme 1, where g_{Gd} is the g-factor for the Gd^{III} ion, H is the applied magnetic field, and $J(\text{Gd}-\text{Gd})$ is the Heisenberg coupling constant between the two adjacent Gd^{III} ions. The best-fit parameters were $g_{Gd} = 1.98$, $J(\text{Gd}-\text{Gd}) = +0.042\ \text{cm}^{-1}$ for **ZnGd1** and $g_{Gd} = 2.01$, $J(\text{Gd}-\text{Gd}) = +0.028\ \text{cm}^{-1}$ for **ZnGd2**, see solid line in Figure 3a and Figure S3 (Supporting Information), indicating a ferromagnetic Gd^{III}–Gd^{III} interaction.

Both ferromagnetic[15] and antiferromagnetic[16] interactions have been observed for binuclear Gd^{III} complexes with small absolute values, below 0.1 cm^{-1}. Previously, we have reported the structures and magnetic properties of two $Ni^{II}_2Gd^{III}_2$ complexes with a similar carbonato-bridged structures, and the best-fit

dx.doi.org/10.1021/ic4022273 | Inorg. Chem. 2013, 52, 12828–12841

parameters of their magnetic susceptibility data gave a small antiferromagnetic (−0.012 cm^{-1}) and a small ferromagnetic (+0.023 cm^{-1}) interaction for Gd^{III}−Gd^{III} interaction.[8] Weak ferromagnetic interaction between Gd^{III}−Gd^{III} ions has been observed for the acetato-bridged binuclear Gd^{III} complex $[\{Gd^{III}(OAc)_3(H_2O)_2\}_2]\cdot 4H_2O$ (OAc = acetato) and phenoxo-bridged binuclear Gd^{III} complex $[Gd^{III}L_3(H_2O)]$ (L = salicylic acid).[15] These coupling constants are comparable to those for our compounds. Recently, the ferromagnetic Gd^{III} cluster with isotropic magnetic property and large magnetocaloric effect (MCE) has attracted much attention in developing molecular refrigerants for liquid-helium temperatures.[17] Evangelisti et al. reported a large value of $-\Delta S_m = 41.6$ J K^{-1} kg^{-1} for ferromagnetic binuclear Gd^{III} complex, $[\{Gd^{III}(OAc)_3(H_2O)_2\}_2]\cdot 4H_2O$. The coupling constant of J = +0.023 cm^{-1} is compatible with those of our carbonato-bridged complexes. The carbonato-bridged Gd^{III} cluster can be a good candidate for the study on MCE.

The magnetization of **ZnGd1** from 0 to 5 T at 1.9 K is shown in Figure 3b, as a plot of $M/N\beta$ vs H. As the magnetic field increases, the magnetization increases saturating to 14.1 and 14.2 $N\beta$ for **ZnGd1** and **ZnGd2** at 5 T, respectively, whose values are compatible with the expected value of 14.0 $N\beta$ for two Gd^{III} species with $S = 7/2$ and $g_{Gd} = 2.00$. Both $M/N\beta$ vs H curves show an intermediate behavior between the Brillouin functions for two isolated spin centers with $S = 7/2$ and for one spin center with $S = 7$. This behavior indicates a weak ferromagnetic interaction between Gd^{III} and Gd^{III} ions in the carbonato-bridged $Zn^{II}_2Gd^{III}_2$ structure and is consistent with the result of the temperature dependence of the magnetic susceptibility.

The ac magnetic susceptibility was measured in a temperature range down to 2.0 K under 0 and 1000 Oe dc fields. The $Zn^{II}_2Gd^{III}_2$ complexes **ZnGd1** and **ZnGd2** showed no frequency-dependent signals down to 2 K in the presence or absence of 1000 Oe bias field, indicating no slow magnetic relaxation (Figure S4, Supporting Information). This is consistent with the static magnetic properties, showing the $Zn^{II}_2Gd^{III}_2$ complexes have a large spin state of $S = 7$ at the ground state due to the Gd^{III}−Gd^{III} ferromagnetic coupling but no magnetic anisotropy due to the Gd^{III} ($4f^7$, $J = 7/2$, $L = 0$, $S = 7/2$, $^8S_{7/2}$) ion.

Magnetic and Luminescent Properties of $Zn^{II}_2Tb^{III}_2$ Complexes. The temperature dependences of dc magnetic susceptibilities in the temperature range of 1.9−300 K and the field dependences of the magnetization at 1.9 K were measured. Figure 4 shows the $\chi_M T$ vs T plots for the $Zn^{II}_2Tb^{III}_2$ complexes **ZnTb1** and **ZnTb2**. The $\chi_M T$ values of **ZnTb1** and **ZnTb2** are 23.33 and 23.04 cm^3 K mol^{-1} per $Zn^{II}_2Tb^{III}_2$ at 300 K, respectively. The ground state for a Tb^{III} ion ($4f^8$, $J = 6$, $S = 3$, $L = 3$, $^7F_6$) is $^7F_6$, with $g_J = 3/2$, separated by more than 2000 cm^{-1} from the first excited state, $^7F_5$, as confirmed by the luminescence spectrum. Indeed, the room-temperature values of $\chi_M T$ are in good agreement with the free ion value 23.64 cm^3 K mol^{-1} for two Tb^{III} ions obtained using the total angular momentum $J = 6$ and the above g_J factor. However, the $^7F_6$ state is split by the crystal field of the ligands, which partially removes the degeneracy of the 13 $|J, J_z\rangle = |6, J_z\rangle$ ($J_z = \pm 6, \pm 5, \pm 4, \pm 3, \pm 2, \pm 1, 0$) components into a series of sublevels (known as Stark splitting) whose width is on the order of 100 cm^{-1}.[18] Therefore, at room temperature, most sublevels are populated and the free ion value is approached. When the temperature is lowered, the $\chi_M T$ value decreases gradually to reach a minimum of 20.04 cm^3 K mol^{-1} at 4.0 K for **ZnTb1** and 20.55 cm^3 K mol^{-1} at 12.0 K **ZnTb2**, respectively, and then increase reaching, respectively, the

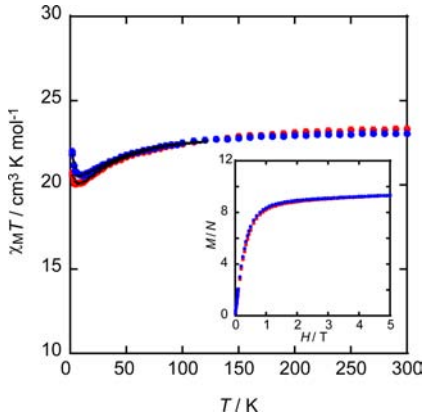

Figure 4. Plots of $\chi_M T$ vs T for the $Zn^{II}_2Tb^{III}_2$ complexes **ZnTb1** (red circles) and **ZnTb2** (blue circles). The solid lines represent the theoretical curves with the best-fit parameters given in the text. (Inset) field dependence of the magnetization at 1.9 K for **ZnTb1** (red circles) and **ZnTb2** (blue circles), as plots of $M/N\beta$ vs H.

values of 20.70 and 21.98 cm^3 K mol^{-1} at 1.9 K. The decrease is mainly due to the crystal field effect on the Tb^{III} ion (vide supra), whereas the increase of $\chi_M T$ value at the lowest temperature region can be ascribed to a weak intramolecular Tb^{III}−Tb^{III} ferromagnetic interaction.

A detailed analysis of the crystal field effect and Tb^{III}−Tb^{III} magnetic coupling on the $\chi_M T$ product would require the diagonalization of a spin Hamiltonian:

$$\mathbf{H} = g\beta(\mathbf{L}_{Tb1} + 2\mathbf{S}_{Tb1})H + g\beta(\mathbf{L}_{Tb2} + 2\mathbf{S}_{Tb2})H + \mathbf{H}_{cf}(Tb_1) + \mathbf{H}_{cf}(Tb_2) - 2J(Tb{-}Tb)\mathbf{J}_{Tb1}\cdot\mathbf{J}_{Tb2} \quad (1)$$

in which the crystal field interaction contribution of each Tb^{III} ion is represented by the equation using the Steven's operators, $\mathbf{H}_{cf} = \Sigma_{K=2,4,6}\Sigma_{q=0}^{K} B_k^q \mathbf{O}_k^q$.[19] Although several excited states and higher-order anisotropy terms, up to the sixth order, should in principle be included in magnetic analysis of lanthanide compounds, the $\chi_M T$ versus T curve in the low temperature range (below 120 K), where only the Stark sublevels of the $^7F_6$ ground state are populated, could be well reproduced considering solely the $^7F_6$ term and including only the quadratic anisotropy terms $\mathbf{O}_2^0$ and $\mathbf{O}_2^2$, as already observed for other Tb^{III} complexes.[3i] Moreover, taking into account the symmetry of the $Zn^{II}_2Tb^{III}_2$ complexes, the two Tb^{III} ions are equivalent and we assumed for them the same anisotropy parameters B_k^q. The temperature dependence of $\chi_M T$ below 120 K was therefore analyzed with the following Hamiltonian:

$$\mathbf{H} = \beta H g_J(\mathbf{J}_{Tb1} + \mathbf{J}_{Tb2}) + B_2^0[\mathbf{O}_2^0(Tb_1) + \mathbf{O}_2^0(Tb_2)] + B_2^2[\mathbf{O}_2^2(Tb_1) + \mathbf{O}_2^2(Tb_2)] - 2J(Tb{-}Tb)\mathbf{J}_{Tb1}\cdot\mathbf{J}_{Tb2} \quad (2)$$

where $\mathbf{O}_2^0 = 3\mathbf{J}_Z^2 - \mathbf{J}^2$ and $\mathbf{O}_2^2 = (\mathbf{J}_+^2 + \mathbf{J}_-^2)/2$, and $\mathbf{H}$ denotes the applied magnetic field, β is the Bohr magneton, B_2^0 and B_2^2 are second-order anisotropy parameters of the Tb^{III} ions, and $J(Tb{-}Tb)$ is the Tb^{III}−Tb^{III} exchange interaction. In our approach, we first carried out a fit of the data in the 16−120 K range, where the Tb^{III}−Tb^{III} interaction is expected to be negligible, to get the g_J, B_2^0, and B_2^2 parameters of the free Tb^{III} ions and then, using the same parameters, we performed a second fit including the $J(Tb{-}Tb)$ exchange interaction for the whole set of data in the 2−120 K range. The fitting parameters so obtained are $g_J = 1.49$, $B_2^0/k_B =$

dx.doi.org/10.1021/ic4022273 | Inorg. Chem. 2013, 52, 12828−12841

−4.5 K, B_2^2/k_B = −0.3 K, and J(Tb−Tb) = +0.0014 cm^{-1} for **ZnTb1** and g_J = 1.50, B_2^0/k_B = −4.6 K, B_2^2/k_B = −0.6 K, and J(Tb−Tb) = +0.0019 cm^{-1} for **ZnTb2**. The theoretical curves are shown as solid lines in Figure 4. It is noted that the g_J values of 1.49 and 1.50 are very close to the theoretical value of 3/2, and the B_2^0 and B_2^2 values for Tb^{III} ion are of the same sign and magnitude of those obtained by Kajiwara et al. for dinuclear Cu^{II}−Tb^{III} complexes with a similar coordination sphere around the Tb^{III} ion.[20]

The diagrams of the multiplet energy levels of the Tb^{III} ions, obtained by diagonalizing only the $\mathbf{O}_2^0$ and $\mathbf{O}_2^2$ terms of Hamiltonian 2, for the two complexes are reported in Figures 5 and S6 (Supporting Information); they are very similar and

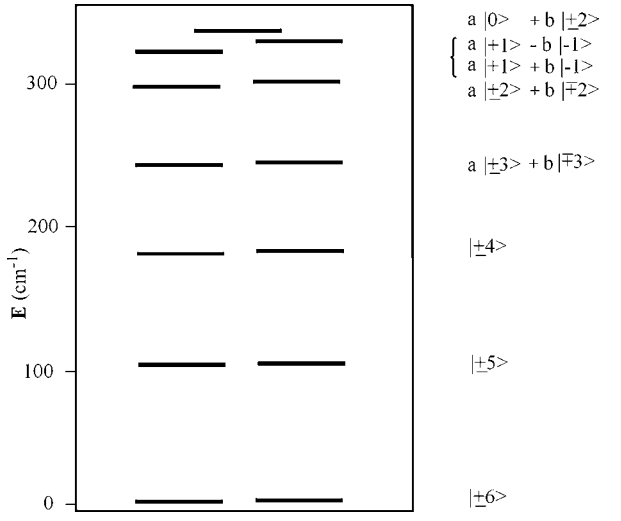

Figure 5. Energy levels of the ground state $^7F_6$ multiplets for the Tb^{III} ion in **ZnTb1** obtained from the magnetic analysis.

only that for **ZnTb1** is discussed. Due to the small size of the transverse term B_2^2, the energy states corresponding to $\pm M_J$ values are almost degenerate except for the ±1 states: the ground state corresponds to an almost pure $|\pm 6\rangle$ with the first excited state, mainly a $|\pm 5\rangle$, at +104 cm^{-1} and the highest multiplet level, a $|0\rangle$ significantly mixed with $|\pm 2\rangle$, at 341 cm^{-1}, which therefore define the total Stark splitting. Such an energy level pattern indicates a strong easy axis (Ising type) anisotropy of the Tb^{III} ion and the presence of a significant barrier for the magnetization reversal, in agreement with the field induced SIM properties of this complex (vide infra).

The field dependences of the magnetization from 0 to 5 T for **ZnTb1** and **ZnTb2** were measured at 1.9 K and the $M/N\beta$ vs H plots are reported in the inset of Figure 4 and show an almost identical behavior. Upon an increase in the applied external magnetic field, the magnetization of $Zn^{II}_2Tb^{III}_2$ complexes increases to 9.33 $N\beta$ at 5 T without reaching the expected saturation value (18 $N\beta$ for two Tb^{III} ions). This is again due to the crystal field effect on the Tb^{III} ion ($4f^8$, J = 6, S = 3, L = 3, $^7F_6$) that removes the 13-fold degeneracy of the $^7F_6$ ground state.

The $Zn^{II}_2Tb^{III}_2$ complexes **ZnTb1** and **ZnTb2** showed an efficient f−f emission in the solid state upon irradiation of UV light at 375 nm. The photograph of the solid sample at room temperature under the irradiation of UV light (365 nm) and the emission spectrum of **ZnTb1** at 77 K is shown in Figure 6, and the emission spectrum of **ZnTb2** is given in Figure S5 (Supporting Information). The emission spectra of binuclear $Zn^{II}Ln^{III}$ complexes with L[1] or similar ligands have recently been

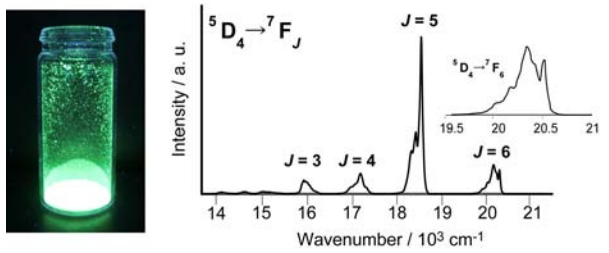

Figure 6. Photograph of the solid sample at room temperature under the irradiation of UV light (365 nm) and emission spectrum of **ZnTb1** by irradiation at 375 nm recorded at 77 K. The fine structure of the $^5D_4 \rightarrow {}^7F_6$ band is shown.

reported,[21] demonstrating this type of ligand can function as appropriate antenna ligand for highly efficient luminescence.[21] The emission bands of **ZnTb1** were observed at ca. 490, 545, 585, and 620 nm and were attributed to the f−f transition $^5D_4 \rightarrow {}^7F_J$ with J = 6, 5, 4, and 3, respectively. Each band exhibited a fine structure with several peaks, corresponding to Stark splitting. For the $^5D_4 \rightarrow {}^7F_6$ transition at 77 K, five peaks were observed at 487.6, 489.6 (sh), 491.8, 496.0 (sh), and 499.8 (sh) nm (i.e., 20.509 × 10^3, 20.425 × 10^3, 20.333 × 10^3, 20.161 × 10^3, and 20.008 × 10^3 cm^{-1} for **ZnTb1**) and five peaks were observed at 487.8, 490.8 (sh), 492.8, 495.8 (sh), and 499.4 (sh) nm (i.e., 20.500 × 10^3, 20.375 × 10^3, 20.292 × 10^3, 20.169 × 10^3, and 20.024 × 10^3 cm^{-1} for **ZnTb2**), which should be correlated with the splitting of the ground $^7F_6$ multiplet. Indeed, the emission spectrum is a direct picture of the ground state Stark multiplet originating from the $^7F_6$ state: the high energy transition of the band corresponds to the transition to the lowest sublevel while the lowest energy transition corresponds to the highest sublevel.

The splitting observed from the emission can be directly compared with the energy diagram obtained from the fitting of the magnetic susceptibility measurements. The comparison for **ZnTb1** is illustrated in Figure 7 and allows to assign the five emission lines of the $^5D_4 \rightarrow {}^7F_6$ band to transitions from the excited $^5D_4$ state to the $|\pm 6\rangle$, $|\pm 5\rangle$, $|\pm 4\rangle$, $|\pm 2\rangle$ and a superposition

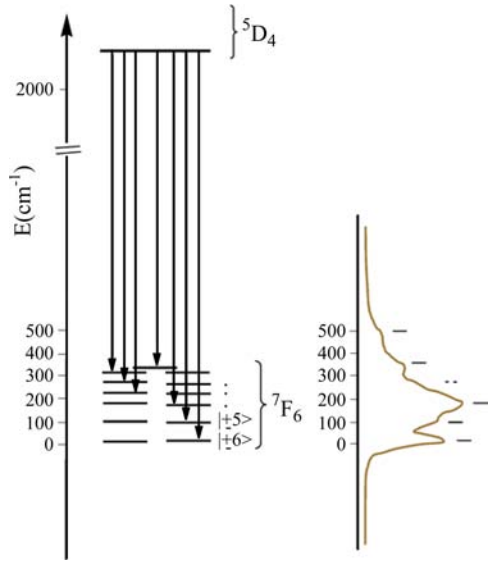

Figure 7. Comparison of the Stark splitting of the $^7F_6$ ground state of the Tb^{III} ions from the magnetic analysis in **ZnTb1** (on the left) and the splitting observed from the emission f−f spectrum (on the right).

dx.doi.org/10.1021/ic4022273 | Inorg. Chem. 2013, 52, 12828−12841

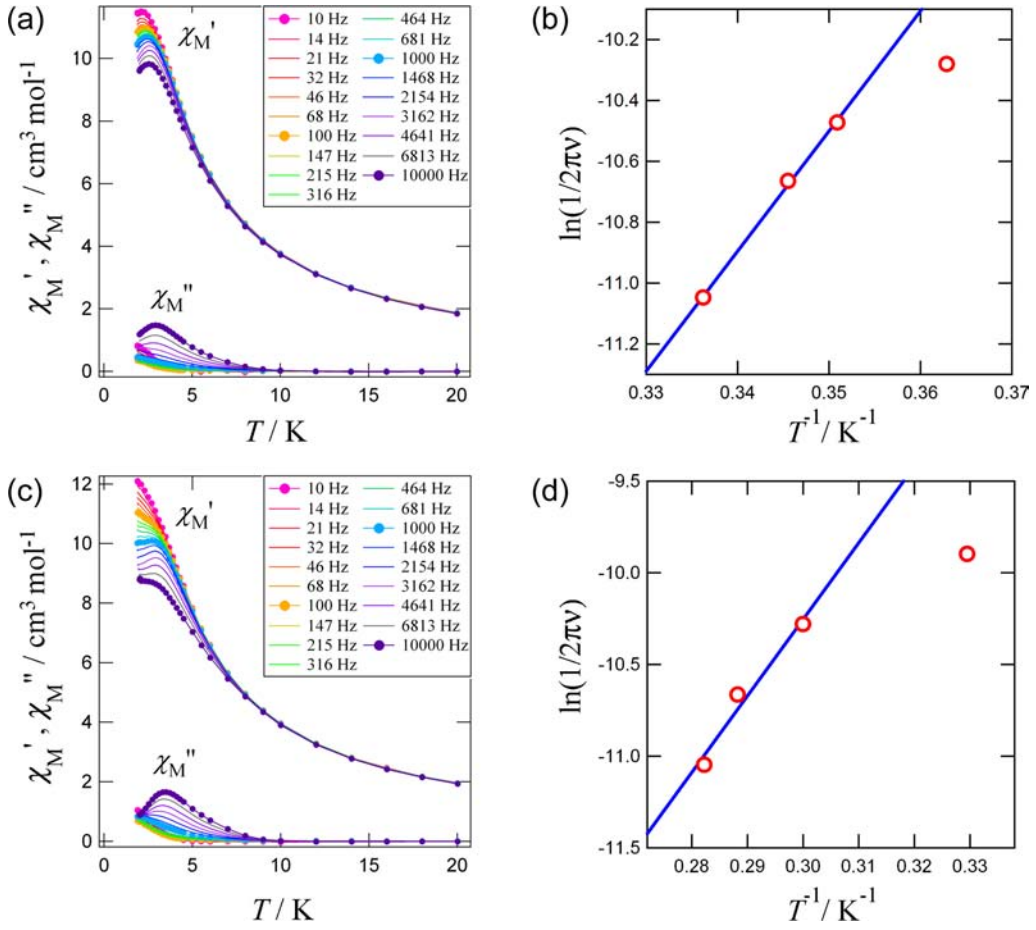

Figure 8. (a) Temperature dependences of the in-phase (χ_M') and out-of phase (χ_M'') ac susceptibility signals of **ZnTb1** measured under various frequencies and under a 1000 Oe external dc field. (b) Arrhenius plots for **ZnTb1**. (c) Temperature dependences of χ_M' and χ_M'' of **ZnTb2** measured under various frequencies and under a 1000 Oe external dc field. (d) Arrhenius plot for **ZnTb2**. For the equation and optimized parameters of the Arrhenius analysis, see the text.

Table 5. ac Magnetic Susceptibility Results on the $Zn^{II}_2Ln^{III}_2$ Complexes

compounds	ZnTb1	ZnTb2	ZnDy1	ZnDy2
H_{dc}	1000	1000	1000	1000
$E_a k_B^{-1}/K^a$	39(1)	42(8)	52(2)	67(2)
τ_0/s^a	$3(1) \times 10^{-11}$	1×10^{-10}	$1.4(4) \times 10^{-8}$	$2.8(9) \times 10^{-9}$
$\alpha_1{}^b$	–	–	0.401(4)	0.320(9)
$\alpha_2{}^c$	–	–	0.105(7)	0.136(10)

[a]From the Arrhenius plot using the χ_M'' peaks. [b]From the Cole–Cole plots measured at 2.0 K. For the equation, see the text. A dash implies that no meaningful Cole–Cole plot has been drawn. [c]From the Cole–Cole plots measured at 5.0 K. For the equation, see the text. A dash implies that no meaningful Cole–Cole plot has been drawn.

of $|\pm1\rangle$ and $|0\rangle$ sublevel, whereas the transition to the $|\pm3\rangle$ multiplet is not well resolved and probably falls on the high energy side of the most intense third emission line, close to the $|\pm2\rangle$ transition. The splitting of the first and second excited sublevel, $|\pm5\rangle$ and $|\pm4\rangle$ (104 and 188 cm^{-1}) fits reasonably well the energy of the second and third emission lines (84 and 176 cm^{-1} above the lowest line at 20.509×10^3 cm^{-1}), whereas the splitting of the highest sublevel are underestimated by ca. 50–150 cm^{-1} as is the total splitting (341 vs 501 cm^{-1}). The comparison for **ZnTb2** (see Figure S7, Supporting Information) is similar with a slightly better agreement for the splitting of the highest excited sublevels and also of the total splitting which, however, remains underestimated (395 vs 476 cm^{-1}). The slight disagreement at higher energies is probably due to their low thermal population at the highest temperature considered in the fitting procedure (120 K), which does not allow their precise localization by thermal variation of the magnetic susceptibility. Nevertheless, the agreement between magnetic and fluorescence properties is reasonably good for the three lowest states, which play the major role in determining the low temperature behavior of these complexes, and confirms that the fine structure of the emission spectrum arises from the splitting of the J_z sublevels of the Tb^{III} ion due to magnetic anisotropy.

The dynamic magnetic properties of the $Zn^{II}_2Tb^{III}_2$ complexes were investigated by using ac magnetic susceptibility measurements. The in-phase (χ_M') and out-of-phase (χ_M'') components exhibit no frequency dependences in a zero bias field but become significantly more intense with the application of an external bias field of 1000 Oe, indicative of SMM. The temperature dependences of the ac magnetic susceptibilities under a 1000

dx.doi.org/10.1021/ic4022273 | Inorg. Chem. 2013, 52, 12828–12841

Oe dc field for **ZnTb1** and the Arrhenius plot are shown in Figure 8a,b, respectively. The activation energy (Δ) for the magnetization reversal using linear temperature region higher than 2.8 K was estimated as $\Delta/k_B = 39(1)$ K with $\tau_0 = 3(1) \times 10^{-11}$ s, where τ_0 stands for the pre-exponential factor in the Arrhenius equation, $\ln(2\pi\nu) = -\ln(\tau_0) - (\Delta/k_B)/T$. The Arrhenius plot shows a deviation from the line in the temperature region less than 2.8 K, indicative of tunneling effect or more than one thermally activated relaxation process. The temperature dependences of the ac magnetic susceptibilities under 1000 Oe dc field for **ZnTb2** and the Arrhenius plot are shown in Figure 8c,d, respectively. A similar Arrhenius analysis on **ZnTb2** gave $\Delta/k_B = 42(8)$ K with $\tau_0 = 1 \times 10^{-10}$ s (Figure 8d). The pre-exponential factors τ_0 of Zn_2Tb_2 complexes are significantly smaller than that of Zn_2Dy_2 complexes (Table 5).

Magnetic Properties of $Zn^{II}_2Dy^{III}_2$ Complexes. The temperature dependences of dc magnetic susceptibilities in the temperature range of 1.9−300 K and the field dependences of the magnetization at 1.9 K were measured. Figure 9 shows the $\chi_M T$ vs

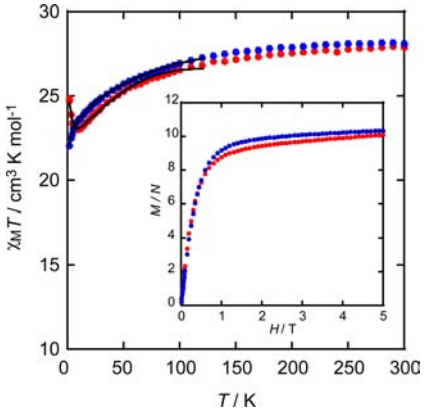

Figure 9. Plots of $\chi_M T$ vs T for the $Zn^{II}_2Dy^{III}_2$ complexes **ZnDy1** (red circles) and **ZnDy2** (blue circles). The solid lines represent the theoretical curves with the best-fit parameters given in the text. (Inset) field dependence of the magnetization at 1.9 K for **ZnDy1** (red circles) and **ZnDy2** (blue circles), as plots of $M/N\beta$ vs H.

T plots for the $Zn^{II}_2Dy^{III}_2$ complexes **ZnDy1** and **ZnDy2**. The $\chi_M T$ values at 300 K for **ZnDy1** and **ZnDy2** are 27.88 and 28.13 cm^3 K mol^{-1}, respectively, whose values are compatible with 28.34 cm^3 K mol^{-1} expected for two noninteracting Dy^{III} ($4f^9$, J = 15/2, S = 5/2, L = 5, g_J = 4/3, $^6H_{15/2}$) ions in the free-ion approximation. When the temperature is lowered, the $\chi_M T$ value of **ZnDy1** decreases gradually to reach a minimum of 23.02 cm^3 K mol^{-1} at 9.0 K, and then increases to 24.85 cm^3 K mol^{-1} at 1.9 K. The decrease in the low temperature region is due to the crystal field effect on the Dy^{III} ion ($4f^9$, $^6H_{15/2}$) that removes the degeneracy of the 16 $|J, J_z\rangle = |15/2, J_z\rangle$ ($J_z = \pm15/2, \pm13/2, \pm11/2, \pm9/2, \pm7/2, \pm5/2, \pm3/2, \pm1/2$) components of the $^6H_{15/2}$ ground state. The increase in the lowest temperature region can be ascribed to the a weak intramolecular Dy^{III}−Dy^{III} ferromagnetic interaction. On the other hand, the $\chi_M T$ value of **ZnDy2** decreases continuously to reach the value of 22.04 cm^3 K mol^{-1} at 1.9 K when the temperature is lowered. The decrease in the low temperature region is mainly due to the crystal field effect on the Dy^{III} ion, and the continuous decrease down to 1.9 K indicates negligible or weak antiferromagnetic Dy^{III}−Dy^{III} interaction (negligible interaction is more likely, vide infra).

The temperature dependence of $\chi_M T$ was analyzed by using the Hamiltonian:

$$\mathbf{H} = \beta H g_J(\mathbf{J}_{Dy1} + \mathbf{J}_{Dy2}) + B_2^0[\mathbf{O}_2^0(Dy_1) + \mathbf{O}_2^0(Dy_2)] + B_2^2[\mathbf{O}_2^2(Dy_1) + \mathbf{O}_2^2(Dy_2)] - 2J(Dy{-}Dy)\mathbf{J}_{Dy1}\cdot\mathbf{J}_{Dy2} \quad (3)$$

and the same two-step approach employed for the analysis of the $Zn^{II}_2Tb^{III}_2$ complexes. The fitting parameters obtained are g_J = 1.26, $B_2^0/k_B = -2.2$ K, $B_2^2/k_B = -1.4$ K, J(Dy−Dy) = +0.0018 cm^{-1} for **ZnDy1** and g_J = 1.28, $B_2^0/k_B = -2.7$ K, $B_2^2/k_B = -1.3$ K, J(Dy−Dy) = −0.0002 cm^{-1} for **ZnDy2**, respectively. The theoretical curves are shown as solid lines in Figure 9. It is noted that the evaluated g_J values of 1.26 and 1.28 are very close to the theoretical value of 4/3, and the B_2^0 and B_2^2 values for Dy^{III} ion are of the same sign and magnitude of those observed in other dinuclear $Zn^{II}Dy^{III}$ complexes.[3i,3j] The difference in the $\chi_M T$ vs T curves of the two compounds at low temperatures is mainly due to different sign of the J(Dy−Dy) coupling constant. The difference is attributed to the slightly different morphology of the ligand field originating from a slightly different arrangement of nitrato ligands around the Dy^{III} ions.

The diagrams of the multiplet energy levels of the Dy^{III} ions, obtained diagonalizing only the $\mathbf{O}_2^0$ and $\mathbf{O}_2^2$ terms of Hamiltonian 3, for **ZnDy1** and **ZnDy2** are reported in Figures 10 and S8

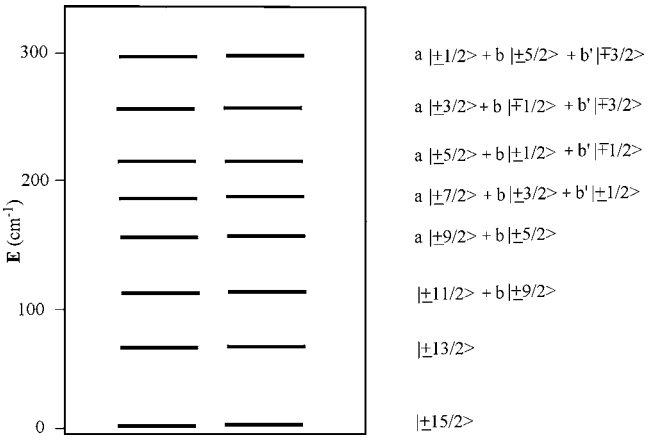

Figure 10. Energy levels of the ground state $^6H_{15/2}$ multiplet for the Dy^{III} ion in **ZnDy1** obtained from the analysis of the dc magnetic susceptibility data.

(Supporting Information); they are similar and only that for **ZnDy1** is discussed. Although the transverse term B_2^2, is higher than in **ZnTb1**, the energy states corresponding to $\pm M_J$ values are still close in energy: the ground state corresponds to an almost pure $|\pm15/2\rangle$ with the first excited state, an almost pure $|\pm13/2\rangle$, at 62 cm^{-1} and the highest multiplet level, $|\pm1/2\rangle$ significantly mixed with $|\pm5/2\rangle$, and to a lesser extent $|\pm3/2\rangle$, at 299 cm^{-1}, which therefore define the total Stark splitting. For **ZnDy2**, a similar energy pattern is evaluated, and the energy separation between the ground state $|\pm15/2\rangle$ and the first excited state $|\pm13/2\rangle$ is 73 cm^{-1}. Such an energy level pattern indicates again strong easy axis anisotropy of the Dy^{III} ion with a significant barrier for the magnetization reversal, in agreement with the SMM properties of this complex (vide infra).

As shown in the inset of Figure 9, upon an increase in the applied external magnetic field, the magnetization of $Zn^{II}_2Dy^{III}_2$ complexes increases to 10.09 and 10.34 $N\beta$ at 5 T for **ZnDy1** and **ZnDy2**, respectively, but did not reach the expected saturation value (20 $N\beta$ for two Dy^{III} ions). This is also due to the crystal

dx.doi.org/10.1021/ic4022273 | Inorg. Chem. 2013, 52, 12828−12841

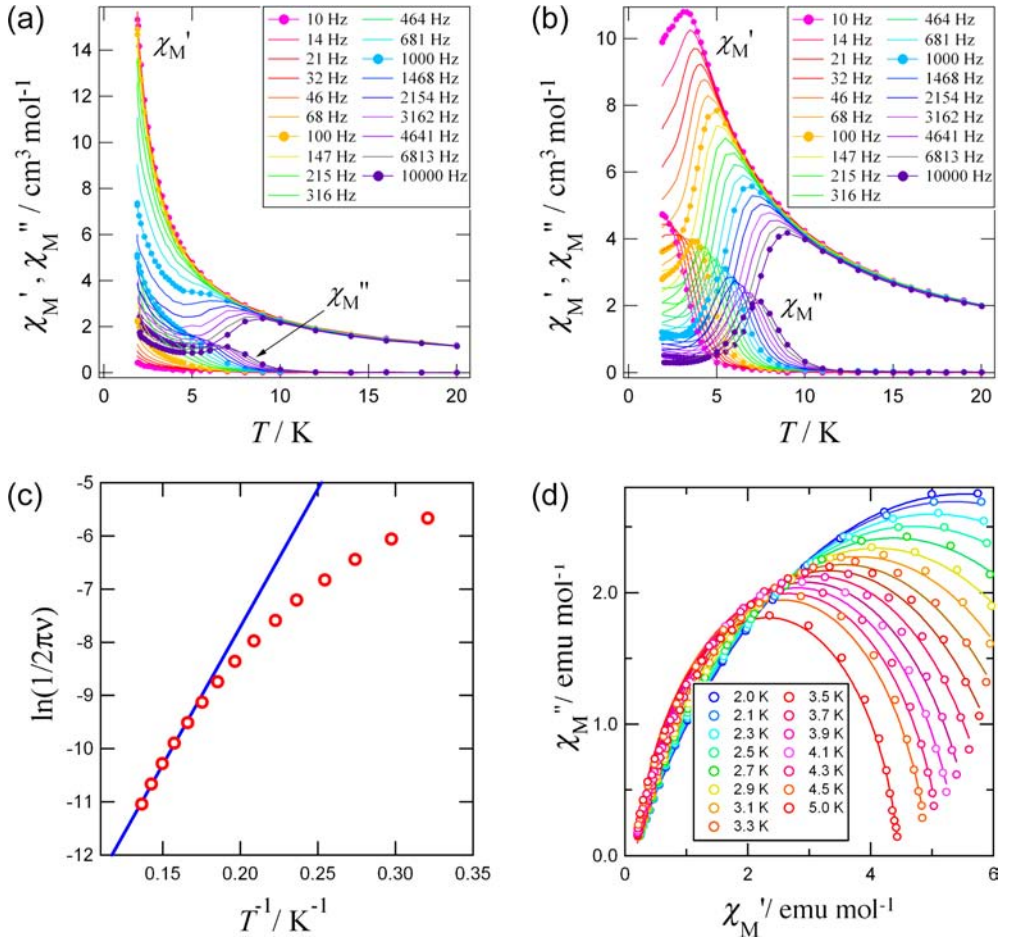

Figure 11. Temperature dependences of the in-phase (χ_M') and out-of-phase (χ_M'') ac susceptibility signals for **ZnDy1** measured under 0 (a) and 1000 Oe (b) dc field. (c) Arrhenius plot and (d) Cole–Cole plots for the data measured at 1000 Oe dc field.

field effect on the Dy^{III} ion ($4f^9$, $J = 15/2$, $S = 5/2$, $L = 5$, $^6H_{15/2}$) that removes the 16-fold degeneracy of the $^6H_{15/2}$ ground state.

The $Zn^{II}_2Dy^{III}_2$ complexes did not show efficient f–f emission spectra in the solid state upon irradiation of UV light at 375 nm. In general, the Dy^{III} complex shows no strong emission. For example, a series of Ln^{III} complexes with the same ligand, $[Ln(hfac)_3PyNO]_2$ (Ln^{III} = Eu, Tb, and Dy; hfac = hexafluoroacetylacetonato, PyNO = pyridine-*N*-oxide), the quantum yields are reported to be 51, 53, and 0.1% for the Eu^{III}, Tb^{III}, and Dy^{III} complexes, respectively.[22] It should be noted that the emission spectra of the binuclear $Zn^{II}Dy^{III}$ complex with a similar Schiff-base ligand (*N*,*N*′-bis(3-methoxysalicylidene)-1,2-ethylenediamine)[21a] and mononuclear Dy^{III} complex of DOTA (DOTA = *N*,*N*′,*N*″,*N*‴-tetraacetic acid-1,4,7,10-tetraazacyclododecane) with the average quantum yield of 1.54% are observed.[23]

The dynamic magnetic properties of the $Zn^{II}_2Dy^{III}_2$ complexes **ZnDy1** and **ZnDy2** were investigated by using ac measurements. For **ZnDy1**, the temperature or frequency dependences of the ac magnetic susceptibilities under 0 and 1000 Oe dc fields were measured, and the results are shown in Figure 11a,b, respectively. The maxima of the in-phase (χ_M') and out-of-phase (χ_M'') components is observed only at a frequency higher than 1500 Hz in a zero bias field but becomes significantly more intense with the application of an external bias field of 1000 Oe. The position of the maxima of the susceptibilities also becomes strongly frequency-dependent, as expected for SMMs. This behavior is probably due to fast zero-field tunneling of the magnetization between sublevels, which is suppressed with the application of the bias field. Such activity is known for SMMs, including Schiff-base systems.[24] To extract the characteristic time and the barrier to relaxation, the relaxation times were fitted by using the Orbach thermally activated relaxation law $\tau = \tau_0 \exp(\Delta/k_BT)$,[1,2] and the Arrhenius plot is shown in Figure 11c. Linear data corresponding to the law were obtained between 6.0 and 7.3 K, with an effective energy barrier of $\Delta/k_B = 52(2)$ K and a relaxation time of $\tau_0 = 1.4(4) \times 10^{-8}$ s in this region. Below 6.0 K, the plots show a departure from the Arrhenius behavior. This suggests that the relaxation might follow a quantum regime below 6.0 K or that there is more than one thermally activated relaxation process present in this system. When we plotted the χ_M'' against χ_M' at various temperatures according to the Cole–Cole analysis (Figure 11d),[24] a semicircle was clearly drawn at each temperature and the α values were obtained. If one relaxation process dominates, the plot will have a semicircular shape with a small value of α. Fitting the data using a generalized Debye model[25] gives a high α value of 0.105(7) at 2 K and 0.401(4) at 5 K, further suggesting that there is likely to be more than one relaxation process operating at high temperatures.

For **ZnDy2**, the temperature or frequency dependences of the ac magnetic susceptibilities under 0 and 1000 Oe dc field are shown in Figure 12a,b, respectively. The in-phase (χ_M') and out-of-phase (χ_M'') components exhibit no frequency dependences in a zero bias field but become significantly more intense with the

dx.doi.org/10.1021/ic4022273 | *Inorg. Chem.* 2013, 52, 12828–12841

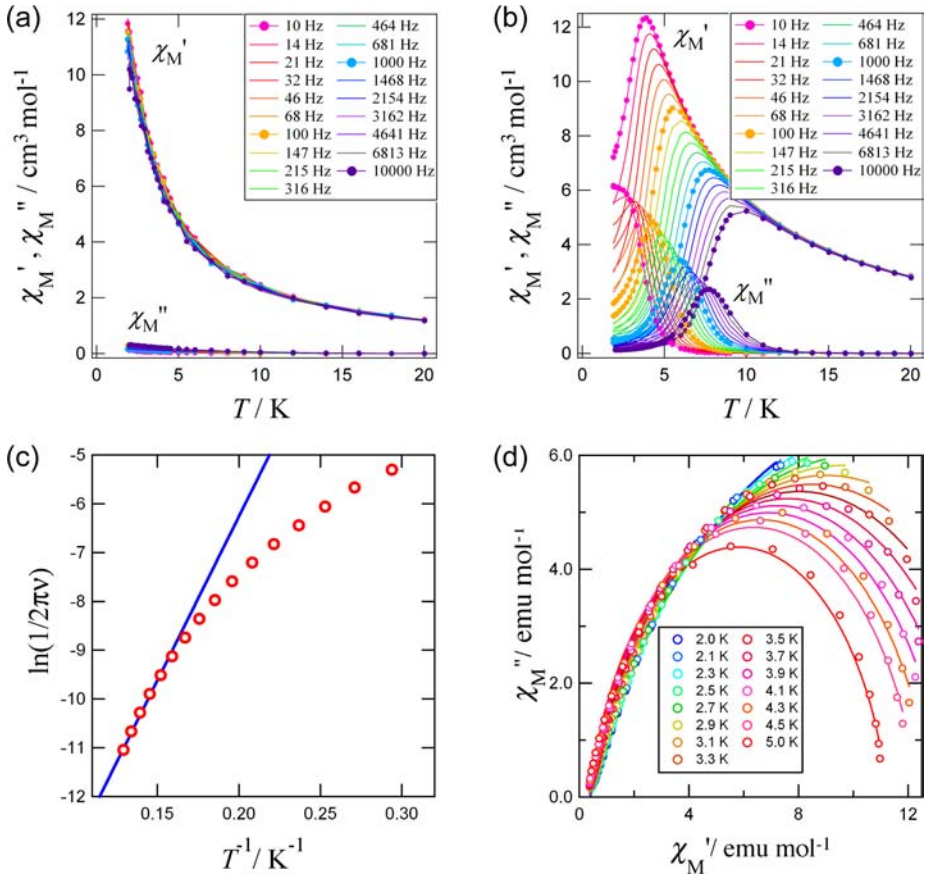

Figure 12. Temperature dependences of the in-phase (χ_M') and out-of-phase (χ_M'') ac susceptibility signals for **ZnDy2** measured under 0 (a) and 1000 Oe (b) dc field. (c) Arrhenius plot and (d) Cole−Cole plots for the data measured at 1000 Oe dc field.

application of an external bias field of 1000 Oe. This behavior is probably due to fast zero-field tunneling of the magnetization between sublevels, which is suppressed with the application of the bias field. The relaxation times were fitted by using the equation $\tau = \tau_0 \exp(\Delta/k_BT)$. Linear data corresponding to the law were obtained between 6.6 and 7.7 K, with an effective energy barrier of $\Delta/k_B = 67(2)$ K and a relaxation time of $\tau_0 = 2.8(9) \times 10^{-9}$ s in this region (Figure 12c). Below 6.6 K, the plots show a departure from the Arrhenius behavior, suggesting a quantum tunneling below 6.6 K or more than one thermally activated relaxation process. The Cole−Cole plots show semicircle at each temperature and the α values were obtained (Figure 12d). The α values of 0.136(10) at 2 K and 0.320(9) at 5 K suggest more than one relaxation process operating at high temperatures.

Comparing Figures 11a and 12a, we can find a significant difference in the SMM performance at a zero dc bias field. The bias field is very effective for disturbing the quantum tunneling of magnetizaiton, as clearly displayed in Figure 12a,b for **ZnDy2**. On the other hand, in Figure 11a for **ZnDy1**, there still appeared the χ_M'' peaks around 7 K even at a zero bias field, though the peak shape was somewhat lowered and broadened. The presence of a small ferromagnetic exchange coupling seems to improve the SMM behavior, because the lanthanide ion senses the exchange bias field within a molecule.[26] Therefore, this finding seems to be in good agreement with the results on the $\chi(T)$ measurements of **ZnDy1** and **ZnDy2** (Figure 9). The former involves an appreciable intramolecular ferromagnetic coupling, whereas the latter lacks any meaningful magnetic coupling.

SMM Parameters of $Zn^{II}_2Ln^{III}_2$ Complexes. Owing to the diamagnetic property of Zn^{II} ion, the magnetic properties of the $Zn^{II}_2Ln^{III}_2$ complexes depend on the nature of the Ln^{III} ion and Ln^{III}−Ln^{III} magnetic interactions and should be compared to those of the $Ni^{II}_2Ln^{III}_2$ complexes of L[1], which exhibit a similar carbonato-bridged structure to $Zn^{II}_2Ln^{III}_2$ complexes and a ferromagnetic interaction between Ni^{II} ($S = 1$) and Ln^{III} ions (Ln^{III} = Gd^{III}, Tb^{III}, Dy^{III}).[8b] The present $Zn^{II}_2Ln^{III}_2$ complexes showed higher Δ/k_B than the $Ni^{II}_2Ln^{III}_2$ complexes (Table 5), indicating that the ferromagnetic Ni^{II}−Tb^{III} and Ni^{II}−Dy^{III} couplings provide a negative effect to the SMM properties, at least for this family of complexes, or in other words the high-spin ground state derived from the ferromagnetic coupling between d- and f-ions does not always improve SMM characteristics. However, this study points out that the presence of a ferromagnetic Ln^{III}−Ln^{III} exchange coupling might positively affect the SMM characteristics by suppressing, or at least decreasing, the zero-field quantum tunneling of the magnetization. Indeed, although a similar frequency dependence of the ac magnetic susceptibilities under 1000 Oe dc bias field was observed for **ZnDy1** and **ZnDy2**, a significant difference was found under the zero bias field where only **ZnDy1**, the only one showing a weak ferromagnetic Dy^{III}−Dy^{III} interaction, has SMM properties.

For **ZnTb1** and **ZnTb2**, the values of the activation barrier estimated from the dynamics of the magnetization are Δ/k_B = 39(1) and 42(8) K, respectively, which are converted to Δ = 27 and 29 cm^{-1}, respectively. These values can be compared with the splitting of the ground sublevel $|\pm6\rangle$ and the first excited

dx.doi.org/10.1021/ic4022273 | Inorg. Chem. 2013, 52, 12828−12841

sublevel $|\pm5\rangle$ evaluated by the magnetic measurement (104 and 128 cm^{-1}) and the energy separation between the lowest and the second emission lines (84 and 125 cm^{-1}). The energy barriers for **ZnDy1** and **ZnDy2** obtained from the Arrhenius plot (Δ/k_B = 52 and 67 K) can be converted to Δ = 36 and 46 cm^{-1}, respectively. These values are close to the calculated Stark energy splitting between the ground and the first excited state (62 and 73 cm^{-1}). These observations suggest that the population of the first excited doublet is sufficient to reverse the magnetization.

■ ASSOCIATED CONTENT

Supporting Information

Crystal packing diagram, temperature dependence of ac magnetic susceptibilities, and luminescent spectrum. X-ray crystallographic files (CIF), and energy levels. This material is available free of charge via the Internet at http://pubs.acs.org. X-ray crystallographic data in CIF format for **ZnGd1**, **ZnTb1**, **ZnDy1** (CCDC 928519−928521) and **ZnGd2**, **ZnTb2**, **ZnDy2** (CCDC 948619−948621) can be obtained via http://www.ccdc.cam.ac.uk/conts/retrieving.html, or from the Cambridge Crystallographic Data Centre, 12 Union Road, Cambridge CB2 1EZ, U.K.; fax (+44) 1223-336-033; or e-mail deposit@ccdc.cam.ac.uk.

■ AUTHOR INFORMATION

Corresponding Author

*N. Matsumoto. E-mail: naohide@aster.sci.kumamoto-u.ac.jp. Fax: +81-96-342-3390.

Notes

The authors declare no competing financial interest.

■ ACKNOWLEDGMENTS

T. Fujinami was supported by the Research Fellowship of the Japan Society for the Promotion of Science, KAKENHI 00248498. This work was carried out under a Core Research Program "Interdisciplinary Chiral Sciences based on Molecular Biology and Chemistry" (Graduate School of Science and Technology, Kumamoto University).

■ REFERENCES

(1) (a) Sessoli, R.; Gatteschi, D.; Caneschi, A.; Novak, M. A. *Nature* **1993**, *365*, 141−143. (b) Gatteschi, D.; Caneschi, A.; Pardi, L.; Sessoli, R. *Science* **1994**, *265*, 1054−1058. (c) Sessoli, R.; Tsai, H. L.; Schake, A. R.; Wang, S.; Vincent, J. B.; Folting, K.; Gatteschi, D.; Christou, G.; Hendrickson, D. N. *J. Am. Chem. Soc.* **1993**, *115*, 1804−1816. (d) Thomas, L.; Lionti, F.; Ballou, R.; Gatteschi, D.; Sessoli, R.; Barbara, B. *Nature* **1996**, *383*, 145−147. (e) Boskovic, C.; Brechin, E. K.; Streib, W. E.; Folting, K.; Bollinger, J. C.; Hendrickson, D. N.; Christou, G. *J. Am. Chem. Soc.* **2002**, *124*, 3725−3736.

(2) (a) Gatteschi, D.; Sessoli, R. *Angew.Chem., Int. Ed.* **2003**, *42*, 268−297. (b) Christou, G. *Polyhedron* **2005**, *24*, 2065−2075. (c) Gatteschi, D.; Sessoli, R.; Villain, J. *Molecular Nanomagnets*; Oxford University Press: Oxford, U.K., 2006. (d) Bagai, R.; Christou, G. *Chem. Soc. Rev.* **2009**, *38*, 1011−1026.

(3) (a) Osa, S.; Kido, T.; Matsumoto, N.; Re, N.; Pochaba, A.; Mronzinski, J. *J. Am. Chem. Soc.* **2004**, *126*, 420−421. (b) Hamamatsu, T.; Yabe, K.; Towatari, M.; Matsumoto, N.; Re, N.; Pochaba, A.; Mrozinski, J. *Bull. Chem. Soc. Jpn.* **2007**, *80*, 523−529. (c) Costes, J.-P.; Dahan, F.; Wernsdorfer, W. *Inorg. Chem.* **2006**, *45*, 5−7. (d) Ferbinteanu, M.; Kajiwara, T.; Choi, K. Y.; Nojiri, H.; Nakamoto, A.; Kojima, N.; Cimpoesu, F.; Fujimura, Y.; Takaishi, S.; Yamashita, M. *J. Am. Chem. Soc.* **2006**, *128*, 9008−9009. (e) Mori, F.; Nyui, T.; Ishida, T.; Nogami, T.; Choi, K.-Y.; Nojiri, H. *J. Am. Chem. Soc.* **2006**, *128*, 14408−14009. (f) Ishida, T.; Watanabe, R.; Fujiwara, K.; Okazawa, A.; Kojima, N.; Tanaka, G.; Yoshii, S.; Noriji, H. *Dalton Trans.* **2012**, *41*, 13609−13619. (g) Gao, Y.; Zhao, L.; Xu, X.; Xu, G.-F.; Guo, Y.-N.; Tang, J.; Liu, Z. *Inorg. Chem.* **2011**, *50*, 1304−1308. (h) Colacio, E.; Ruiz, J.; Mota, A. J.; Palacios, M. A.; Cremades, E.; Ruiz, E.; White, F. J.; Euan K. Brechin, E. K. *Inorg. Chem.* **2012**, *51*, 5857−5868. (i) Efthymiou, C. G.; Stamatatos, T. C.; Papatriantafyllopoulou, C.; Tasiopoulos, A. J.; Wernsdorfer, W.; Perlepes, S. P.; Christou, G. *Inorg. Chem.* **2010**, *49*, 9737−9739. (j) Burrow, C. E.; Burchell, T. J.; Lin, P.-H.; Habib, F.; Wernsdorfer, W.; Clérac, R.; Murugesu, M. *Inorg. Chem.* **2009**, *48*, 8051−8053. (k) Yamaguchi, T.; Sunatsuki, Y.; Ishida, H.; Kojima, M.; Akashi, H.; Re, N.; Matsumoto, N.; Pochaba, A.; Mrozinski, J. *Bull. Chem. Soc. Jpn.* **2008**, *81*, 598−605. (l) (c) Hamamatsu, T.; Yabe, K.; Towatari, M.; Osa, S.; Matsumoto, N.; Re, N.; Pochaba, A.; Mrozinski, J.; Gallani, J. L.; Barla, A.; Imperia, P.; Paulsen, C.; Kappler, J. P. *Inorg. Chem.* **2007**, *46*, 4458−4468. (m) Sessoli, R.; Powell, A. K. *Coord. Chem. Rev.* **2009**, *253*, 2328−2341. (n) Costes, J. P.; Vendier, L.; Wernsdorferc, W. *Dalton Trans.* **2011**, *40*, 1700−1706.

(4) (a) Ishikawa, N.; Sugita, M.; Ishikawa, T.; Koshihara, S.; Kaizu, Y. *J. Am. Chem. Soc.* **2003**, *125*, 8694−8695. (b) Ishikawa, N.; Sugita, M.; Okubo, T.; Tanaka, N.; Iino, T.; Kaizu, Y. *Inorg. Chem.* **2003**, *42*, 2440−2446. (c) Woodruff, D. N.; Winpenny, R. E. P.; Layfield, R. A. *Chem. Rev.* **2013**, *113*, 5110−5148. (d) Habib, F.; Murigesu, M. *Chem. Soc. Rev.* **2013**, *42*, 3278−3288.

(5) (a) Sorace, L.; Benelli, C.; Gatteschi, D. *Chem. Soc. Rev.* **2011**, *40*, 3092−3104. (b) Layfield, R. A.; McDouall, J. J. W.; Sulway, S. A.; Tuna, F.; Collison, D.; Winpenny, R. E. P. *Chem.—Eur. J.* **2010**, *16*, 4442−4446. (c) Long, J.; Habib, F.; Lin, P.-H.; Korobkov, I.; Enright, G.; Ungur, L.; Wernsdorfer, W.; Chibotaru, L.; Murugesu, M. *J. Am. Chem. Soc.* **2011**, *133*, 5319−5328. (d) Guo, Y.-N.; Xu, G.-F.; Guo, Y.; Tang, J. *Dalton Trans.* **2011**, *40*, 9953−9963. (e) Hewitt, I. J.; Tang, J.; Madhu, N. T.; Anson, C. E.; Lan, Y.; Luzon, Y.; Etienne, M.; Sessoli, R.; Powell, A. K.. *Angew. Chem., Int. Ed.* **2010**, *49*, 6352−6356. (f) Blagg, R. J.; Muryn, C. A.; McInnes, E. J. L.; Tuna, F.; Winpenny, R. E. P. *Angew. Chem., Int. Ed.* **2011**, *50*, 6530−6533. (g) Rhinehart, J. D.; Feng, M.; Evans, W. J.; Long, J. R. *J. Am. Chem. Soc.* **2011**, *133*, 14236−14239. (h) Zhang, P.; Guo, Y.-N.; Tang, J. *Coord. Chem. Rev.* **2013**, *257*, 1728−1763. (I) Luzon, J.; Sessoli, R. *Dalton Trans.* **2012**, *41*, 13556−13567.

(6) (a) Lin, P.-H.; Burchell, T. J.; Clerac, R.; Murugesu, M. *Angew. Chem., Int. Ed.* **2008**, *47*, 8848−8851. (b) Hewitt, I. J.; Lan, Y.; Anson, C. E.; Luzon, J.; Sessoli, R.; Powell, A. K. *Chem. Commun.* **2009**, 6765−6767. (c) Guo, Y.-N.; Xu, G.-F.; Wernsdorfer, W.; Ungur, L.; Guo, Y.; Tang, J.; Zhang, H.-J.; Chibotaru, L. F.; Powell, A. K. *J. Am. Chem. Soc.* **2011**, *133*, 11948−11951. (d) Zhang, P.; Zhang, L.; Lin, S.-Y.; Tang, J. *Inorg. Chem.* **2013**, *52*, 6595−6602.

(7) (a) Ke, H.; Zhao, L.; Xu, G.-F.; Guo, Y.-N.; Tang, J.; Zhang, X.-Y.; Zhang, H.-J. *Dalton Trans.* **2009**, 10609−10613. (b) Bian, S.-D.; Jia, J.-H.; Wang, Q.-M. *J. Am. Chem. Soc.* **2009**, *113*, 3422−3423. (c) Langley, S. K.; Moubaraki, B.; Murray, K. S. *Inorg. Chem.* **2012**, *51*, 3947−3949. (d) Tian, H.; Zhao, L.; Guo, Y. N.; Guo, Y.; Tang, J.; Liu, Z. *Chem. Commun.* **2012**, *48*, 708−710. (e) Vallejo, J.; Cano, J.; Gastro, L.; Julve, M.; Loret, F.; Fabelo, O.; Canadillas-Delgado, L.; Pardo, E. *Chem. Commun.* **2012**, *48*, 7726−7728. (f) Titos-Padilla, S.; Ruiz, J.; Herrera, J. M.; Brechin, E. K.; Wersndorfer, W.; Lloret, F.; Colacio, E. *Inorg. Chem.* **2013**, *52*, 9620−9626.

(8) (a) Sakamoto, S.; Yamauchi, S.; Hagiwara, H.; Matsumoto, N.; Sunatsuki, Y.; Re, N. *Inorg. Chem. Commun.* **2012**, *26*, 20−23. (b) Sakamoto, S.; Fujinami, T.; Nishi, K.; Matsumoto, N.; Mochida, N.; Ishida, T.; Sunatsuki, Y.; Re, N. *Inorg. Chem.* **2013**, *52*, 7218−7229.

(9) (a) Gruber, S. J.; Harris, C. M.; Sinn, E. *J. Inorg. Nucl. Chem.* **1968**, *30*, 1805−1830. (b) Towatari, M.; Nishi, K.; Fujinami, T.; Matsumoto, N.; Sunatsuki, Y.; Kojima, M.; Mochida, N.; Ishida, T.; Re, N.; Mrozinski, J. *Inorg. Chem.* **2013**, *52*, 6160−6178.

(10) (a) Murase, M.; Yamauchi, S.; Sakamoto, S.; Takahashi, S.; Matsumoto, N.; Tsuchimoto, M. *Polyhedron* **2013**, *59*, 76−84. (b) Yamauchi, S.; Hashibe, T.; Murase, M.; Hagiwara, H.; Matsumoto, N.; Tsuchimoto, M. *Polyhedron* **2013**, *49*, 105−112.

(11) Kahn, O. *Molecular Magnetism*; VCH: Weinhein, 1993. Chapter 1, Table I.1.

(12) Sheldrick, G. M. *SHELXL-97*; University of Göttingen: Göttingen, Germany, 1997.
(13) *CrystalStructure* 3.7.0, single crystal structure analysis software; Rigaku and Rigaku/MSC: The Woodlands, TX, 2000−2005.
(14) Nakamoto, K. *Infrared and Raman Spectra of Inorganic and Coordination Compounds*, 2nd ed.; Wiley-Interscience: New York, 1970; p 98.
(15) (a) Panagiotopoulos, A.; Zafiropoulos, T. F.; Perlepes, S. P.; Bakalbassis, E.; Masson-Ramade, I.; Kahn, O.; Terzis, A.; Raptopoulou, C. P. *Inorg. Chem.* **1995**, *34*, 4918−4920. (b) Rohde, A.; Urland, W. J. *Z. Anorg. Allg. Chem.* **2005**, *631*, 417−420. (c) Hatscher, S. T.; Urland, W. *Angew. Chem., Int. Ed.* **2003**, *42*, 2862−2864. (d) Baggio, R.; Calvo, R.; Garland, M. T.; Pena, O.; Perec, M.; Rizzi, A. *Inorg. Chem.* **2005**, *44*, 8979−8987.
(16) (a) Rizzi, A.; Baggio, R.; Calvo, R.; Garland, M. T.; Peña, O.; Perec, M. *Inorg. Chem.* **2001**, *40*, 3623−3625. (b) Cañadillas-Delgado, L.; Fabelo, O.; Pasan, J.; Delgado, F. S.; Lloret, F.; Julve, M.; Ruiz-Perez, C. *Dalton Trans.* **2010**, *39*, 7286−7293. (c) Cañadillas-Delgado, L.; Pasán, J.; Fabelo, O.; Julve, M.; Lloret, F.; Ruiz-Pérez, C. *Polyhedron* **2013**, *52*, 321−332.
(17) (a) Evangelisti, M.; Roubeau, O.; Palacios, E.; Camòn, A.; Hooper, T. N.; Brechin, E. K.; Alonso, J. J. *Angew. Chem., Int. Ed.* **2011**, *50*, 6606−6609. (b) Sessoli, R. *Angew. Chem., Int. Ed.* **2012**, *51*, 43−45.
(18) (a) Kajiwara, T.; Nakano, M.; Takahashi, K.; Takaishi, S.; Yamashita, M. *Chem.—Eur. J.* **2011**, *17*, 196−205. (b) Yamaguchi, T.; Sunatsuki, Y.; Ishida, H.; Kojima, M.; Akashi, H.; Re, N.; Matsumoto, N.; Pochaba, A.; Mrozinski, J. *Inorg. Chem.* **2008**, *47*, 5736−5745.
(19) Stevens, K. W. H. *Proc. Phys. Soc., London, Sect. A* **1952**, *A65* (3), 209−215.
(20) Kajiwara, T.; Nakano, M.; Takaishi, S.; Yamashita, M. *Inorg. Chem.* **2008**, *47*, 8604−8606.
(21) (a) Pasatoiu, T. D.; Tiseanu, C.; Madalan, A. M.; Jurca, B.; Duhayon, C.; Sutter, J. P.; Andruh, M. *Inorg. Chem.* **2011**, *50*, 5879−5889. (b) Yamashita, K.; Miyazaki, R.; Kataoka, Y.; Nakanishi, T.; Hasegawa, Y.; Nakano, M.; Yamamura, T.; Kajiwara, T. *Dalton Trans.* **2013**, *42*, 1987−1990.
(22) Yi, X.; Bernot, K.; Pointillart, F.; Poneti, G.; Calvez, G.; Daiguebonne, C.; Guillou, O.; Sessoli, R. *Chem.—Eur. J.* **2012**, *18*, 11379−11387.
(23) (a) Long, J.; Vallat, R.; Ferreira, R. A. S.; Carlos, L. D.; Paz, F. A. A.; Guari, Y.; Larionova, J. *Chem. Commun.* **2012**, *48*, 9974−9976. (b) Cucinotta, G.; Perfetti, M.; Luzon, J.; Etienne, M.; Car, P.-E.; Caneschi, A.; Calvez, G.; Bernot, K.; Sessoli, R. *Angew. Chem., Int. Ed.* **2012**, *51*, 1606−1610.
(24) Luzon, J.; Sessoli, R. *Dalton. Trans.* **2012**, *41*, 13556−13567.
(25) Cole, K. S.; Cole, H. R. *J. Chem. Phys.* **1941**, *9*, 341−351.
(26) (a) Rinehart, J. D.; Long, J. R. *Chem. Sci.* **2011**, *2*, 2078−2085. (b) Murakami, R.; Ishida, T.; Yoshii, S.; Nojiri, H. *Dalton Trans.* **2013**, *42*, 13968−13973 and references therein.